Disturbed engram network caused by NPTXs downregulation underlies aging-related memory deficits

Tao Jin[1,2,3], Yang Yang[1,2,3], Yu Guo[1,3], Yi Zhang[1], Qiumin Le[1,2], Nan Huang[1,2], Xing Liu[1,2], Jintai Yu[1], Lan Ma[1,2]* and Feifei Wang[1,2]*

[1] State Key Laboratory of Medical Neurobiology and MOE Frontiers Center for Brain Science, Institutes of Brain Science, School of Basic Medical Sciences, Department of Neurology and National Center for Neurological Disorders, Huashan Hospital, Fudan University, Shanghai 200032, China.

[2] Research Unit of Addiction Memory, Chinese Academy of Medical Sciences (2021RU009), Shanghai 200032, China.

[3] These authors contributed equally: Tao Jin, Yang Yang, Yu Guo

*Corresponding author. Email: lanma@fudan.edu.cn and ffwang@fudan.edu.cn

Abstract

Engram cells storing specific memories are allocated to separate neuronal ensembles, which preferentially recruit either excitatory or inhibitory inputs to drive precise memory expression. However, how these formed neuronal ensembles maintain their stability, and whether the disturbed stability contributes to aging-related memory deficits remain elusive. Here, we show that neuronal pentraxin1 (NPTX1) facilitates Kv7.2-mediated inhibition of *Fos*$^+$ ensemble hyperexcitability, thereby restricting its response to excitatory inputs from medial entorhinal cortex (MEC) and promoting memory expression in the fear context. Meanwhile, NPTX2 facilitates the perisomatic inhibition of the *Npas4*$^+$ ensemble by parvalbumin$^+$ (PV$^+$) interneurons, thus preventing fear memory overgeneralization. Pharmacological activation of Kv7.2 or chemogenetic activation of PV$^+$ interneurons repaired memory deficits caused by engram specific NPTXs depletion. Contextual fear memory precision and NPTXs expression in dentate gyrus (DG) engram cells are decreased in aged mice. Overexpression of NPTX1 in *Fos*$^+$ ensemble or AMPAR binding domain of NPTX2 in *Npas4*$^+$ ensemble rescued memory imprecision. These findings elucidate that the coordination of NPTXs prevents engram ensembles from becoming hyperactive and provide a causal link between engram network destabilization and aging-associated memory deficits.

Key Words: Engram stability, NPTXs, aging, memory deficits

Introduction

Memories are believed to be encoded in sparse neuronal ensembles (engram cells) that are activated by specific learning experiences[1,2]. Neurons recruited to engrams are more stably connected than those that are not[3]. Memory accessibility and precision are shaped by the plasticity of engram network, and require the long-lasting stabilization of the recruited engram network. However, the molecular mechanisms underlying the maintenance of the dormant, but stable engram network remain unknown. In addition, memory precision progressively declines with age, and is considered as one of the predominant hallmarks of aging-associated cognitive dysfunctions[4,5], while it remains to be elucidated how the disturbed engram network leads to aging-related memory deficits.

Cell-adhesion molecules (CAMs) are a super family which play an irreplaceable role in synaptic plasticity through mediating the bidirectional organization of synaptic compartments[6]. NPTXs are a subfamily of CAMs primarily expressed in excitatory neurons. NPTXs consist of NPTX1, NPTX2 and their receptor NPTXR[7]. Pre-synaptic secreted NPTX1 and NPTX2 form disulfide-linked heteromultimers with post-synaptic NPTXR to promote the clustering of α-amino-3-hydroxy-5-methyl-4-isoxazolepropionic acid (AMPA) type glutamate receptors (AMPARs)[8,9]. Further studies identify NPTX1 functions as a pro-apoptotic protein[10] that restricts excitatory synaptic transmission[11]. In contrast, NPTX2 maintains excitatory homeostasis by adaptively enhancing circuit inhibition[12,13]. These findings raise the possibility that NPTX1 and NPTX2 function as the potential molecular substrates for stabilizing the

excitatory and inhibitory inputs onto distinct neuronal ensembles. NPTXs are also considered as prognostic biomarkers for neurodegeneration whose expressions are decreased in Alzheimer's disease (AD), schizophrenia or even mild cognitive impairment (MCI) patients[14-16]. However, the causal link between NPTXs reduction-induced engram network destabilization and aging-related memory deficits remain unclear.

The tracing of neuronal circuits involved in specific memory formation is enabled by measuring the expression of selectively activated immediate early genes (IEGs). The DG engram cells within the equivalent memory contain functionally divergent *Fos*$^+$ and *Npas4*$^+$ neuronal ensembles, which drive precise memory expression by recruiting excitatory and inhibitory (E/I) circuits[17]. The expression of NPTX1 and NPTX2 are both abundant in DG[18]. In this study, we found that the maintenance of engram network stability requires NPTX1 and NPTX2 to coordinately stabilize the excitatory inputs to the *Fos*$^+$ ensemble and the inhibitory inputs to the *Npas4*$^+$ ensemble. Engram network hyperactivity, caused by NPTXs downregulation in DG engram ensembles contributed to aging-related contextual fear memory imprecision, including impaired memory expression in the fear context and overgeneralization in the non-fear context, which was rescued by restoring NPTXs expression in different engram ensembles. Our findings elucidate the critical role of NPTXs in stabilizing the formed engram network by controlling DG excitatory and inhibitory inputs, and establish a causal link between engram network destabilization and aging-associated memory deficits.

Results

NPTX1 restricts MEC excitatory inputs onto DG *F*-RAM ensemble

Fos and *Npas4*-dependent robust activity marking (*F*-RAM and *N*-RAM) reporter systems were used to label engram ensembles with mKate2 reporter by off Dox[17]. *Npas4-CreER*^{T2} mice in which the endogenous *Npas4* promoter drives the expression of *CreER*^{T2} were generated to label *Npas4*$^{+}$ ensembles with EGFP reporter by 4-hydroxytamoxifen (4-OHT) intraperitoneal (i.p.) injection (Figure. S1A-1D). A combination of these two activity-dependent labelling strategies (Figure. S1E) was used simultaneously to label engrams activated by contextual fear conditioning (CFC, 0.5 mA, 1 s, 3 trials). The EGFP^{+} neurons showed substantial overlap with mKate2^{+} *N*-RAM ensemble while showed minimal colocalization with mKate2^{+} *F*-RAM ensemble (Figure. S1F-1G). These results confirm that *Fos*$^{+}$ and *Npas4*$^{+}$ engram cells in DG labeled by *F*-RAM and *N*-RAM reporters are distinct populations.

The upstream inputs of *F*- and *N*-RAM neuronal ensembles from medial septum (MS), horizontal limb of the diagonal band (HDB), perirhinal cortex (PRh), lateral entorhinal cortex (LEC), medial entorhinal cortex (MEC) and DG were detected by rabies virus (RV) tracing (Figure 1A-1B). *F*-RAM ensemble formed more connections with MS and MEC, while *N*-RAM ensemble received more inputs from DG local neurons (Figure 1C). The majority of dsRed^{+} neurons in MS were co-labelled with the cholinergic neuron marker choline acetyltransferase (ChAT, Figure 1D-1E), and DG *F*-RAM neurons received more excitatory inputs from MEC than *N*-RAM neurons (Figure 1F-1G).

98 NPTXs were found to be predominantly involved in E/I synaptic homeostasis rather
99 than cholinergic signaling[9,19]. To test whether NPTXs modulate the stability of the
100 synaptic transmission between MEC and DG *Fos*$^{+}$ ensemble, *Nptx1*$^{fl/fl}$, *Nptx2* $^{fl/fl}$
101 conditional knockout (*Nptx1* cKO, *Nptx2* cKO) mice were generated (Figure S2A-2B).
102 Ribosome-associated transcripts of *F*-RAM and *N*-RAM ensembles were enriched
103 from *Nptxs* cKO mice and their WT littermates (Figure S2C-2D), and qPCR against
104 *Nptx1* exon 3 and *Nptx2* exon 2 was performed to confirm the knockout efficiency in
105 *F*- or *N*-RAM ensembles. *Nptx2* expression was unaffected when *Nptx1* was depleted
106 and vice versa (Figure S2E-2L). Immunostaining of NPTX1 and NPTX2 further
107 confirmed the knockout efficiency in DG engram ensembles (Figure S3).
108 *AAV-CaMKIIα-ChR2-mCherry* was then injected into MEC of *Nptx1* cKO, *Nptx2* cKO
109 mice and their WT littermates, and the virus mixture of *AAV-F-RAM-Cre* with Cre
110 recombinase-dependent *AAV-DIO-H2B-EGFP* was injected into DG to knock out *Nptxs*
111 in *Fos*$^{+}$ ensemble. Opto-evoked excitatory post-synaptic currents (oEPSCs) from MEC
112 were recorded on EGFP^{-} (*F*-RAM^{-}) and EGFP^{+} (*F*-RAM^{+}) cells (Figure 1H). The
113 amplitude of oEPSCs on EGFP^{+} cells was larger in the *Nptx1* cKO group (Figure 1I-
114 1J), whereas this effect was not found in the *Nptx2* cKO mice (Figure 1K-1L). These
115 data indicate that NPTX1 plays an important role in dampening the excitatory synaptic
116 transmission between MEC and DG *Fos*$^{+}$ ensemble.
117

118 **NPTX1 facilitates I_M current and membrane expression of Kv7.2 in DG *F*-RAM**
119 **ensemble**

Action potential (AP) recordings were performed to examine whether neuronal excitability of the engram ensembles was changed after *Nptxs* knockout (Figure 2A-2C). *F*-RAM engram cells lacking *Nptx1,* but not *Nptx2,* exhibited upward shift of the neuronal spiking curve after step-increment current injections, lower resting membrane potential (RMP) and rheobase (Figure 2D-2K), indicating increased excitability of *F*-RAM engram cells after *Nptx1* knockout. KCNQ2 (Kv7.2) pairs with the KCNQ3 (Kv7.3) subunit to form KCNQ2/3 heterotetramers, which are the primary molecular substrate of M-current (I_M) involved in regulating neuronal excitability[20,21]. Application of the KCNQ2/3-selective blocker XE991 resulted in a reduction of I_M amplitude on DG *F*-RAM engram cells (Figure 2L-2M). *Nptx1* depletion exerted the similar inhibitory effect of XE991 on I_M amplitude (Figure 2N-2O). Co-immunoprecipitation (Co-IP) of the DG lysate confirmed the interaction between NPTX1 and Kv7.2 (Figure 2P). Immunostaining analysis further revealed that *Nptx1* ablation decreased Kv7.2 membrane expression in *F*-RAM engram cells (Figure 2Q-2R), which was not observed in *Nptx2* cKO group (Figure 2S-2T). Taken together, these results indicate that NPTX1 restrains the excitatory synaptic transmission between MEC and DG *Fos*$^+$ ensemble by facilitating Kv7.2 membrane expression-mediated inhibition of neuronal hyperexcitability.

NPTX2 in *N*-RAM ensemble facilitates the perisomatic inhibition by PV$^+$ interneurons in DG

Rabies tracing confirmed *N*-RAM ensemble received more inputs from DG local

142 neurons (Figure 1C), leading us to wonder whether NPTX2 was specifically involved
143 in *Npas4*$^{+}$ engram-DG local neuron synaptic connection. Immunostaining showed that
144 parvalbumin^{+} (PV^{+}) and somatostatin^{+} (SST^{+}) interneurons, two major subtypes of
145 GABAergic interneurons in DG[22] that separately target perisomatic compartments and
146 distal apical dendrites of granule cells[23] were both recruited by DG *Fos*$^{+}$ and *Npas4*$^{+}$
147 engram cells after CFC. However, *Npas4*$^{+}$ engram cells received more PV^{+} but not
148 SST^{+} inputs in DG (Figure 3A-3B, Figure S4A-4B).
149 To test the involvement of NPTX2 in the synaptic transmission between *N*-RAM
150 ensemble and DG interneurons, the viral mixture of *AAV-N-RAM-Cre, AAV-DIO-ChR2-*
151 *EYFP, AAV-PV/SST-Flp* and Flp recombinase-dependent *AAV-fDIO-mCherry* was
152 injected into DG of *Nptx1* cKO, *Nptx2* cKO mice and WT littermates. The specificity
153 of *AAV-SST-Flp* and *AAV-PV-Flp* was confirmed by immunostaining with anti-SST and
154 anti-PV antibodies (Figure S4C-4D, Figure S5A). Opto-evoked paired-pulse ratio (PPR)
155 and AMPAR/N-methyl-D-aspartate receptor (NMDAR) (A/N) ratio were recorded on
156 SST^{+} or PV^{+} interneurons according to mCherry expression, morphology and location
157 (Figure 3C-3D, Figure S4E-4F). *Nptxs* depletion in *N*-RAM ensemble reduced pre-
158 synaptic glutamate release (Figure S4G-4H, S4K-4L, Figure S5B-5E,), consistent with
159 previous studies that NPTXs family promotes pre-synaptic glutamate release[19,24]. *Nptx2*
160 knockout in *N*-RAM ensemble exerted no effect on A/N ratio of SST^{+} interneurons
161 (Figure S4I-4J, S4M-4N), whereas *Nptx2,* but not *Nptx1* depletion in *N*-RAM ensemble
162 significantly decreased AMPAR-mediated EPSC and A/N ratio on PV^{+} interneurons
163 (Figure 3E-3J). Previous studies found that NPTX2 binds AMPAR subunit GluA4 on

164 PV^+ interneurons to regulate network excitatory/inhibitory balance[12,25].
165 Immunostaining confirmed that *Nptx2* depletion in *N*-RAM ensemble decreased the
166 expression of GluA4 on PV^+ interneurons (Figure 3K-3L).
167 To examine whether NPTX2-dependent plasticity applies to GABAergic CCK^+ cells,
168 the viral mixture of *AAV-N-RAM-Cre, AAV-DIO-ChR2-EYFP* with *AAV-vGAT2-Flp-*
169 dependent expression of *AAV-CCK-fDIO-mCherry* was injected into DG of WT and
170 *Nptx2* cKO mice to label the GABAergic CCK^+ cells (Figure S6A-6C). Opto-evoked
171 PPR and A/N ratio were recorded on $mCherry^+$ interneurons, and no differences were
172 detected after *Nptx2* depletion in *N*-RAM ensemble (Figure S6D-6G). These data
173 suggest that NPTX2-dependent interneuron plasticity was specific to PV^+ interneurons.
174 The disturbed PV^+ interneuron plasticity caused by *Nptx2* depletion led us to speculate
175 whether the inhibitory inputs received by *N*-RAM ensemble was also affected. A viral
176 mixture of *AAV-fDIO-ChR2-mCherry*, *AAV-N-RAM-Cre* and *AAV-Flex-EGFP-Nptx2*
177 *shRNA (Nptx2 sh)* was injected into DG of *PV-Flpe* mice, and opto-evoked inhibitory
178 post-synaptic currents (oIPSCs) and PPR were recorded on *N*-RAM cells (Figure 3M-
179 3N). The increased PPR in the *Nptx2 shRNA* group indicates the reduction of pre-
180 synaptic γ-aminobutyric acid (GABA) release from PV^+ interneurons (Figure 3O-3P),
181 leading to the reduced inhibition $Npas4^+$ engram cell received (Figure 3Q-3R). Taken
182 together, these data indicate that NPTX2 facilitates the inhibitory synaptic transmission
183 between DG $Npas4^+$ engram cells and PV^+ interneurons by the AMPAR-dependent
184 mechanism.
185

186 **NPTX1 in DG *F*os$^+$ ensemble and NPTX2 in DG *Npas4*$^+$ ensemble facilitate the**
187 **precise expression of contextual fear memory**

188 To investigate the involvement of NPTXs-dependent maintenance of engram network
189 stability on behavioral outputs, the viral mixture of *AAV-F-RAM-Cre* or *AAV-N-RAM-*
190 *Cre* combined with *AAV-DIO-EYFP* was injected into DG of young *Nptx1* cKO, *Nptx2*
191 cKO mice and their respective WT littermates. Mice were tested on day 3 in context A
192 and context C after fear conditioning (Figure 4A-4C, 4H-4J). The freezing level during
193 conditioning was not different between *Nptx1* cKO, *Nptx2* cKO mice and their WT
194 littermates (Figure S7A-7D). Interestingly, *Nptx1* depletion in *F*-RAM ensemble
195 decreased freezing in context A (Figure 4D-4E), whereas *Nptx2* depletion in *F*-RAM
196 neuronal ensemble caused no differences in freezing level in both contexts (Figure 4F-
197 4G). *Nptx1* knockout in DG *N*-RAM ensemble did not affect the freezing level in either
198 context (Figure 4K-4L), whereas *Nptx2* knock out in DG *N*-RAM ensemble increased
199 the freezing level in the non-fear context C on day 3, indicating overgeneralization of
200 contextual fear memory (Figure 4M-4N).

201 In addition, when mice were exposed to a novel context (context N) quite different with
202 context A or context C, *Nptx1* or *Nptx2* was knocked out in randomly labeled *F*- or *N*-
203 RAM neurons (Figure 4O-4Q), and no differences in freezing were found between
204 *Nptxs* cKO and WT controls (Figure S7E-7F, Figure 4R-4U), indicating the fear
205 context-specific effect of *Nptxs*. Moreover, *Nptxs* depletion in both ensembles had no
206 effect on mice's locomotion, anxiety or depression levels (Figure S8-S10).

207 Taken together, these data suggest that the precise expression of contextual fear memory,

208 including high freezing level in the fear context but low freezing level in the non-fear
209 context requires the coordination of NPTX1 and NPTX2 functioning in distinct
210 ensembles.
211

212 **Pharmacological activation of Kv7.2 or chemogenetic activation of PV$^+$**
213 **interneurons ameliorates memory deficits induced by NPTXs depletion in DG**
214 **engrams**

215 The Kv7.2 activator retigabine, a clinically used anticonvulsant[26], was i.p. injected 30
216 min before mice were tested in the fear context A and non-fear context C (Figure 5A-
217 5C). Retigabine had no effect on the freezing level of WT mice in either context,
218 whereas it restored the reduced freezing level in context A when NPTX1 was depleted
219 in *F*-RAM ensemble but not in *N*-RAM ensemble (Figure 5D-5G, Figure S11A-11B).
220 To rescue memory overgeneralization induced by *Nptx2* knockout in *N*-RAM ensemble,
221 the designer receptors exclusively activated by designer drugs (DREADDs) were used
222 to activate PV$^+$ interneurons. The viral mixture of *AAV-N-RAM-Cre*, *AAV-Flex-EGFP-*
223 *Nptx2 shRNA* and *AAV-fDIO-hM3Dq-mCherry* was injected into the DG of *PV-Flpe*
224 mice and clozapine N-oxide (CNO) was administrated by i.p. injection 30 min before
225 the mice were tested in context A and context C (Figure 5H-5J). Chemogenetic
226 activation of local DG PV$^+$ interneurons had no effect on the freezing level of control
227 group infected with *Scramble shRNA*, while it reduced the freezing level of mice in
228 context C when *Nptx2* was knocked down in *N*-RAM ensemble instead of *F*-RAM
229 ensemble (Figure 5K-5N, Figure S11C-11D).

230

231 **Downregulation of NPTX1 and NPTX2 in DG engrams or human cerebrospinal**

232 **fluid (CSF) was correlated with cognitive deficits**

233 Maladaptive changes in the expression of functional synaptic protein leading to

234 neuronal network destabilization and cognitive impairment, are central hallmarks

235 associated with physiological brain aging[27]. NPTXs are considered as biomarkers of

236 synaptic dysfunction and cognitive impairment[7,16]. To investigate whether *Nptxs*

237 expression in DG changes during physiological aging, young (3m) and aged (18m) mice

238 were sacrificed 15 min, 30 min, 60 min and 120 min after CFC or under homecage (HC)

239 condition, smFISH was used to assess their mRNA expression (Figure 6A-6D, S12A-

240 12D).

241 *Fos*$^+$ and *Npas4*$^+$ cell numbers after CFC were decreased in the DG of aged mice,

242 especially at 30 and 60 min, indicating decreased activation of neurons during learning

243 in aged mice (Fig S12E-12F). *Nptx1* was expressed in all DG granule cells, although

244 the overall *Nptx1*$^+$ fluorescence intensity was not significantly decreased in aged mice

245 (Figure 6E), the specific expression of *Nptx1* in *Fos*$^+$ and *Npas4*$^+$ engram cells were

246 reduced (Figure 6F, Figure S12G). NPTX2 was also seen as a neuronal IEG protein[14],

247 both *Nptx2*$^+$ cell numbers and the average fluorescence intensity of *Nptx2 mRNA* in

248 *Fos*$^+$ and *Npas4*$^+$ engram cells were decreased in aged mice (Figure 6G-6H, Figure

249 S12H). These findings indicate the downregulation of *Nptx1* and *Nptx2* in *Fos*$^+$ and

250 *Npas4*$^+$ engram cells in aged mice.

251 The expression of contextual fear memory in young and aged mice were further

252 assessed. When exposed to strong fear conditioning (0.5 mA, 1 s, 3 trials), aged mice
253 froze more in the non-fear context C, suggesting memory overgeneralization (Figure 6I,
254 6K-6L). However, when exposed to mild fear conditioning (0.3 mA, 1 s, 1 trial), aged
255 mice froze less in the fear context A (Figure 6J, 6M-6N), suggesting memory retrieval
256 impairment. These results demonstrate that aging impairs the precise expression of
257 contextual fear memory.
258 To investigate whether NPTX1 and NPTX2 expression were associated with
259 longitudinal changes of clinical cognitive scores, correlations between NPTXs in
260 human CSF of cognitively normal (CN) and MCI individuals from the Alzheimer's
261 Disease Neuroimaging Initiative (ADNI) database and cognition were analyzed. The
262 reduction of NPTXs exhibited significant associations with accelerated deterioration in
263 global cognition scores, including the Clinical Dementia Rating-Sum of Boxes
264 (CDRSB) and Mini-Mental State Examination (MMSE) as well as in executive and
265 language function (Figure 6O-6P). These clinical data confirmed that CSF NPTXs can
266 be a strong prognostic biomarker of accelerated cognitive decline with potential use as
267 a therapeutic target.
268
269 **NPTXs overexpression in DG engrams rescued memory deficits in aged mice**
270 Consistent with the decreased number of *Fos*$^{+}$ and *Npas4*$^{+}$ cells in DG after CFC, the
271 number of cells labelled by the *F*- and *N*-RAM systems were both reduced in DG of
272 aged mice (Figure S12I-12J). Ribosome-associated transcripts of *F*-RAM and *N*-RAM
273 ensembles activated in the home cage or by CFC were analyzed (Figure S13A). Gene

274 ontology (GO) analysis revealed clusters of differentially expressed genes (DEGs)
275 related to synaptic plasticity and cell communication between *F*-RAM and *N*-RAM
276 ensembles, which were more significant after CFC (Figure S13B). In addition, a
277 minority of DEGs overlapped between *F*- and *N*-RAM ensembles during aging (Figure
278 S13C-13D). DEGs in *F*-RAM during aging were preferentially enriched in pathways
279 regulating neuronal excitability, including membrane potential and potassium ion
280 import, whereas DEGs in *N*-RAM during aging were preferentially enriched in
281 AMPAR-mediated glutamatergic transmission and others (Figure S13E), suggesting
282 different pathways involved in engram network plasticity during aging between *F*- and
283 *N*-RAM ensembles.
284 Decreased Kv7.2 membranes expression on c-Fos$^+$ engram cells (Figure 7A-7B) and
285 NPTX1-Kv7.2 interaction in DG (Figure 7C-7D, S14A) were observed in aged mice.
286 AAV-DIO-Nptx1-EYFP was constructed to overexpress NPTX1 in a Cre-dependent
287 way (Figure S14B). Aged mice were subjected to the mild fear conditioning protocol
288 (0.3 mA, 1 s, one shock). Overexpression of NPTX1 in *F*-RAM ensemble, but not in
289 *N*-RAM ensemble increased the freezing level of aged mice in the fear context A
290 (Figure 7E-7K, Figure S14C-14D). Decreased GluA4 expression on PV$^+$ interneurons
291 and PV$^+$ fluorescence intensity surrounding Npas4$^+$ engram cells were observed in aged
292 mice (Figure 7L-7O), which are consistent with the phenotype of *Nptx2* depletion in
293 young mice (Figure 3). Aged mice overexpressing the AMPAR binding domain of
294 NPTX2 (NPTX2-PTX)[18] in *N*-RAM ensemble, but not in *F*-RAM ensemble rescued
295 overgeneralization in context C during retrieval (Figure 7P-7V, Figure S14E-14F).

296 However, overexpression of NPTX1 and NPTX2-PTX in young mice had no effect on
297 freezing levels when tested in either context A or context C (Figure S15). These data
298 confirm that DG engram network hyperactivity caused by NPTXs downregulation
299 underlies aging-associated memory imprecision, and that re-stabilization of NPTX1-
300 dependent MEC-*Fos*$^+$ engram excitatory circuit and NPTX2-dependent DG PV$^+$
301 interneuron-*Npas4*$^+$ engram inhibitory circuit is able to repair memory deficits in aged
302 mice.
303

304 **Discussion**

305 Contextual learning activates distinct *Fos*$^+$ and *Npas4*$^+$ engram ensembles, recruiting
306 enhanced excitatory and inhibitory circuits respectively to modulate memory-guided
307 adaptive behaviors. However, fundamental questions still remain: how the recruited
308 engram network maintains its stability and whether aging-related memory imprecision
309 associates with engram network destabilization. Our study identified NPTXs as the
310 molecular substrates that prevent network hyperactivity and maintain memory
311 precision. Although the NPTXs expression are not specific to *Fos*$^+$ and *Npas4*$^+$ engram
312 cells, the functional specificity of NPTXs should be placed into specific engram circuits
313 to be manifested, and the maintenance of circuit stability depends on the stable
314 expression of NPTX1 and NPTX2 specifically. Molecules and circuits, they are
315 interdependent, both are essential for ensuring precise behavioral outputs.

316 NPTX1 plays a critical role in stabilizing the excitatory synaptic connection between
317 MEC and DG *Fos*$^+$ engram cells via facilitating Kv7.2 membrane expression-

318 dependent inhibition of neuronal hyperexcitability to promote memory retrieval. Our
319 data demonstrate that NPTX1 interacts with a specific potassium channel Kv7.2 *in vivo*,
320 although it might not be a direct interaction and probably requires other auxiliary
321 proteins such as syntaxin[28], we provide a possible explanation for NPTX1 to regulate
322 neuronal excitability beyond its classical role in glutamate signaling. Our behavioral
323 output caused by *Nptx1* depletion in *F*-RAM ensemble was inconsistent with the results
324 of Sun *et al*[17] that chemogenetic activation of *F*-RAM ensemble or optogenetic
325 inhibition of MEC-DG circuit promoted or inhibited memory generalization. That's
326 probably because chemogenetic or optogenetic manipulation was transient, while *Nptx1*
327 depletion somehow mimics the persistent activation, leading to engram
328 hyperexcitability and decreased the signal-to-noise ratio (SNR) of MEC-*Fos*$^+$ ensemble
329 excitatory transmission during memory retrieval. Besides, a number of studies support
330 the view that MEC inputs onto DG regulate memory retrieval[29,30].
331 NPTX2 stabilizes the inhibitory synaptic connection between DG local PV$^+$
332 interneurons and *N*-RAM ensemble to suppress memory overgeneralization, consistent
333 with Sun *et al*'s report that *N*-RAM ensemble contributed to memory discrimination[17].
334 Their finding confirmed the involvement of CCK$^+$ interneurons, while our finding
335 illustrated the importance of NPTX2 in mediating PV$^+$ interneurons plasticity. We
336 speculate that *N*-RAM ensemble-dependent mediation of memory discrimination may
337 require the coordination of both CCK$^+$ and PV$^+$ GABAergic interneurons as they have
338 been found to exert complementary roles in recruiting perisomatic inhibition[31,32] while
339 NPTX2 specifically regulates the functional connection between PV$^+$ interneurons and

340 *Npas4*$^{+}$ engram cells. NPTX2 was found as a downstream protein of NPAS4[33,34], which
341 explained the coincidence of the weakened perisomatic inhibition caused by *Nptx2*
342 knockout with the finding of *Npas4* depletion by Elizabeth A *et al*'s [35]. As a neuronal
343 IEG, Npas4 upregulates perisomatic inhibitory synapses when activated,[34,36] to scale
344 down the level of network activity in response to neuronal excitation, but the specific
345 mechanism remains to be elucidated. Our study provide the downstream molecular
346 mechanism for Npas4 activation-dependent mediation of memory precision. The
347 specificity of NPTX2 functions in *Npas4*$^{+}$ ensemble but not in *Fos*$^{+}$ ensemble to
348 regulate memory discrimination can also be supported by the study by Ee-Lynn *et al*
349 that knockdown of *Nptx2* in *Fos*$^{+}$ ensemble had no effect on the perisomatic inhibition
350 received from PV^{+} interneurons[37].
351 Memory precision changes dynamically across the lifespan, young individuals only
352 form gist-like memories and slowly develop into precise episodic memories as the brain
353 matures, then the ability to retrieve specific information declines with age.
354 Understanding the maladaptive changes in the engram network stability during aging
355 may provide insights to combat aging-induced cognitive deficits. NPTXs are classic
356 synaptic proteins that may also be prognostic biomarkers in cognitive and mental
357 disorders, such as AD and schizophrenia[14,15]. *Nptx2* was also seen as a neuronal IEG.
358 Our smFISH results showed that the total number of *Nptx2*$^{+}$ cells and the expression of
359 *Nptx2* in engram cells were both downregulated in DG during aging, whereas the
360 overall downregulation of *Nptx1* was not observed in aged mice, indicating that NPTX2
361 was more sensitive to aging. That is to say, along with aging, *Nptx2* downregulation-

362 induced disruption of local perisomatic inhibition of DG engram occurs before *Nptx1*
363 downregulation-induced disruption of MEC-DG engram excitatory long-range
364 projection, which probably explains why generalization always occurs before amnesia
365 in aged individuals. The findings of Ramsaran *et al* showed that extracellular
366 perineuronal nets-dependent functional maturation of PV^+ interneurons promotes
367 sparse engram formation and memory precision during brain development[38]. Our study
368 elucidated that engram network hyperactivity, caused by NPTXs downregulation
369 contributes to aging-related memory imprecision and provided potential synaptic and
370 molecular strategies to mitigate different phenotypes of aging-related memory
371 imprecision, such as amnesia and overgeneralization respectively.

372 **Data availability**

373 ADNI data are publicly available to bona fide researchers upon application at
374 https://adni.loni.usc.edu/. The *F*- and *N*-RAM engram cells RNA-seq data have been
375 submitted to NCBI Gene Expression Omnibus (GEO) under accession number
376 PRJNA1067898.

377 **Code availability**

378 Custom codes will be provided upon request.

379 **Acknowledgement**

380 This work was supported by grants from the STI2030-Major Projects (2021ZD0203500
381 to FFW and LM, 2021ZD0202100 to XL), the Natural Science Foundation of China
382 (32222033 to FFW, 31930046 and 82021002 to LM, 32171041 to XL, 31970543 and
383 32270660 to QML), the CAMS Innovation Fund for Medical Sciences (2021-I2M-5-

009 to LM and XL). We thank Prof. Yingxi Lin (The University of Texas Southwestern Medical Center, Texas, USA) for providing the *AAV-Fos-RAM-d2tTA-TRE-mKate2* and *AAV-Npas4-RAM-d2tTA-TRE-mKate2* plasmids. The human data used in this study were obtained from the ADNI (http://adni.loni.usc.edu/) database. The authors thank all participants who donated their brains to the ADNI Neuropathology Core Center. The authors also thank all investigators who collected and processed specimens and performed neuropathological assessments in ADNI. As such, the investigators within the ADNI contributed to the design and implementation of the database and/or provided data but did not participate in the analysis or the writing of this paper. A complete listing of ADNI investigators can be found at: http://adni.loni.usc.edu/wpcontent/uploads/how_to_apply/ADNI_Acknowledgement_List.pdf. We express appreciation to contributors of the ADNI database. Data collection and sharing for this project was funded by the ADNI (National Institutes of Health Grant U01 AG024904) and DOD ADNI (Department of Defense award number W81XWH12-2-0012). ADNI is funded by the National Institute on Aging, the National Institute of Biomedical Imaging and Bioengineering, and through generous contributions from the following: AbbVie, Alzheimer's Association; Alzheimer's Drug Discovery Foundation; Araclon Biotech; BioClinica, Inc.; Biogen; BristolMyers Squibb Company; CereSpir, Inc.; Cogstate; Eisai Inc.; Elan Pharmaceuticals, Inc.; Eli Lilly and Company; EuroImmun; F. HoffmannLa Roche Ltd and its affiliated company Genentech, Inc.; Fujirebio; GE Healthcare; IXICO Ltd.; Janssen Alzheimer Immunotherapy Research & Development, LLC; Johnson & Johnson Pharmaceutical

Research & Development LLC; Lumosity; Lundbeck; Merck & Co., Inc.; Meso Scale Diagnostics, LLC; NeuroRx Research; Neurotrack Technologies; Novartis Pharmaceuticals Corporation; Pfizer Inc.; Piramal Imaging; Servier; Takeda Pharmaceutical Company; and Transition Therapeutics. The Canadian Institutes of Health Research is providing funds to support ADNI clinical sites in Canada. Private sector contributions are facilitated by the Foundation for the National Institutes of Health (www.fnih.org). The grantee organization is the Northern California Institute for Research and Education, and the study is coordinated by the Alzheimer's Therapeutic Research Institute at the University of Southern California. ADNI data are disseminated by the Laboratory for Neuro Imaging at the University of Southern California.

Author contributions

F.W., L.M. and T.J. designed the research. T.J. and Y.Y. conducted the AAV vector construction, virus injection, immunostaining, Co-IP, smFISH, Ribo Tag purification and the behavioral experiments. T.J. carried out the electrophysiology recordings. T.J., N.H., Y.Y. and Q.L. contributed to the bioinformatics analysis. T.J., Y.Y. and X.L. analyzed the data and T.J. carried out the statistical analysis and drafted the manuscript. Y.G. and Y. Z. analyzed the clinical data and J.Y. supervised these data. L.M. and F.W. supervised the project and revised the paper.

Competing interests

The authors declare no competing financial interests.

Methods

Study population

428 The data for human samples were obtained from the ADNI database
429 (http://adni.loni.usc.edu/). The ADNI project is a multicenter longitudinal study that
430 recruits participants from more than 50 sites across the United States and Canada. It
431 was initiated as a public-private partnership in 2003 with the primary goal of
432 continuously collecting clinical, genetic, imaging, biological, and neuropsychological
433 data to evaluate the progression of MCI and early AD dementia. The ADNI study has
434 obtained approval from the Institutional Review Boards of all participating centers.
435 Written informed consent has been derived from all participants.
436 For all ADNI participants, standardized assessments were carried out and diagnoses
437 were made based on normative study criteria for either control, MCI, or AD dementia.
438 Detailed diagnostic criteria can be accessed at www.adni-info.org. In brief, the CN
439 controls were defined as having a MMSE score of at least 24 and a Clinical Dementia
440 Rating (CDR) score of 0. MCI participants showed MMSE scores between 24 and 30,
441 objective memory loss tested by delayed recall of the Wechsler Memory Scale Logical
442 Memory II, a CDR score of 0.5, preserved activities of daily living, and no dementia.
443 For the purpose of analysis, we included a total of 570 non-demented subjects
444 (comprised of 167 CN controls and 403 MCI patients) whose CSF proteomic assay data
445 were available at baseline.

446 **CSF protein measurement**

447 The baseline CSF sample collection was completed at each ADNI study site and stored
448 in a -80°C freezer. Samples were shipped on dry ice to the laboratory of Washington
449 University School for proteomic analysis. Quantification was undertaken using the

450 Slow Offrate Modified Aptamer (SOMAmer)-based capture array method, where the
451 SomaScan platform captures specific protein targets using chemically synthesized
452 SOMAmer reagents. The high reliability of the SOMAscan approach for detecting
453 protein levels has been proven in previous studies, with an overall median coefficient
454 of variation of approximately 5% within and between plates[39,40]. Protein measurements
455 were performed following the routine SomaScan data standardization, normalization,
456 and quality control procedures (https://ida.loni.usc.edu/). Assay details have been
457 previously described[39]. The ADNI cohort releases data from 7,008 analytes that map to
458 6,361 unique proteins. All CSF protein levels were reported in relative fluorescence
459 units (RFU). In this study, we extracted only aging-related CSF proteins from the ADNI
460 database for analysis.

461 **Cognitive assessments**

462 The CDR-SB and MMSE scores were used to indicate global cognitive ability. The
463 ADNI composite scores reflecting memory (MEM), executive function (EF), language
464 (LAN), and visuospatial function (VS) were used to perform cognitive domain
465 evaluations[41].

466 **Animals**

467 All animals used in this study were listed as follows: adult C57BL/6J male mice (3 m)
468 from the SLAC Laboratory Animal Company (Shanghai, China), aged C57BL/6J male
469 mice (16-18 m) from the Aniphe Biolaboratory Inc. (Nanjing, China) and *PV-Flpe*
470 (021191) mice from the Jackson Laboratory (CA, USA). CRISPR-Cas9 mediated
471 construction of *Nptx1*$^{fl/fl}$, *Nptx2*$^{fl/fl}$ conditional knockout (*Nptx1* cKO, *Nptx2* cKO) mice

472 targeting exon 3 and exon 2 respectively were generated by the Biocytogen Co. (Beijing,
473 China) and *Npas4-CreER*^{T2} mice were generated by Shanghai Model Organisms center,
474 Inc (Shanghai, China). *Npas4-CreER*^{T2} and *PV-Flpe* mice were bred to C57BL/6J mice
475 for more than six generations, *Nptx1*$^{fl/fl}$, *Nptx2*$^{fl/fl}$ mice and their respective wild-type
476 (WT) littermates were obtained from self-crossing of *Nptx1*$^{fl/+}$, *Nptx2*$^{fl/+}$ (heterozygous)
477 mice. Genotypes were determined by polymerase chain reaction (PCR) of mouse toe
478 DNA samples. The primers for genotyping PCR were as follows: 5' -
479 GCTGTAGGGATGCTTGTCTCTGGTG - 3' and 5' -
480 AGAAAAGCTGACCCAAGGTCTCTGC - 3' for *Nptx1 5' loxP,* 5' -
481 ATTAGCTGCCAGATCTTAGCCCCCT - 3' and 5' -
482 GTGTGTGTCCCTGGTGGTGAAGTTT - 3' for *Nptx1 3' loxP,* 5' -
483 GAATGGCTCGAGGCAGGTCCAGTTT - 3' and 5' -
484 CGTTACTAAACCCCAGACAGCTCCG - 3' for *Nptx2 5' loxP,* 5' -
485 AGTTCTGCCTCTGTTCATCTTGCCA - 3' and 5' -
486 TTCACCTGACCCTTCTGTTCACGAC - 3' for *Nptx2 3' loxP,* 5' -
487 AGAGCCTGAGCGAAAAGACC - 3', 5' - CTGCTCACCTCCAGCAAAGA - 3' and
488 5' - CGCGCGCCTGAAGATATAGA - 3' for *Npas4-CreER*^{T2}. Male offsprings at 8-12
489 weeks of age were used in following experiments, which were randomly assigned to
490 groups. All mice were housed on a 12 hr light/dark cycle (light on from 8 a.m. to 8 p.m.)
491 with access to food and water *ad libitum*. All experiment procedures were strictly in
492 accordance with the National Institutes of Health Guide for the Care and Use of
493 Laboratory Animals, and were approved by Animal Care and Use Committee of the

494 animal facility at Fudan University.

495 **Viral vectors**

496 *AAV-Fos-RAM-d2tTA-TRE-mKate2* and *AAV-Npas4-RAM-d2tTA-TRE-mKate2*
497 plasmids were kind gifts from Prof. Yingxi Lin (The University of Texas Southwestern
498 Medical Center, Texas, USA). To generate *AAV-Fos-RAM-d2tTA-TRE-Cre* and *AAV-*
499 *Npas4-RAM-d2tTA-TRE-Cre* plasmids, *mKate2* in *AAV-Fos-RAM-d2tTA-TRE-mKate2*
500 and *AAV-Npas4-RAM-d2tTA-TRE-mKate2* plasmids was replaced with the *Cre*
501 sequence obtained by PCR from *pAAV-Cre-GFP* (Addgene: 68544). *pAAV-CMV-*
502 *bGlobin-Flex-EGFP-MIR30-Scramble-shRNA*, *pAAV-CMV-bGlobin-Flex-EGFP-*
503 *MIR30-Nptx2-shRNA* and *pAAV-CMV-DIO-Nptx2-PTX-P2A-EGFP* were used in our
504 previous paper[18]. To generate *pAAV-Ef1α-DIO-Nptx1-T2A-EYFP*, the coding sequence
505 for mouse *Nptx1* with *T2A* was generated by Azenta US, Inc. (Suzhou, China) and was
506 subcloned into *pAAV-Ef1α-DIO-EYFP* (Addgene: 27056). Adeno-associated viruses
507 (AAVs) described above were packaged by OBiO Technology Co., Ltd (Shanghai,
508 China) into serotype 9. *AAV_9-Ef1α-Flex-NBL10* (69971) and *AAV_9-Ef1α-DIO-ChR2-*
509 *EYFP* (S0199-9-H50) were purchased from Taitool Bioscience Co., Ltd. (Shanghai,
510 China). *AAV_9-Ef1α-DIO-H2B-EGFP* (PT-0258), *AAV_9-Ef1α-DIO-EYFP* (PT-0012),
511 *AAV_9-CaMKIIα-ChR2-mCherry* (PT-0297), *AAV_9-VGAT2-Flp* (PT-2501, vector
512 backbone from BrainVTA), *AAV_9-CCK-fDIO-mCherry* (PT-8508, vector backbone
513 from Addgene: 114471), *AAV_8-Ef1α-DIO-TVA-H2B-EGFP* (PT-0021), *AAV_8-Ef1α-*
514 *DIO-RVG* (PT-0023) and *RV-ENVA-ΔG-dsRed* (R01002) were purchased from
515 BrainVTA Co., Ltd. (Wuhan, China). *AAV_9-PV-Flp* (BC-0430, vector backbone from

516 Addgene: 22914), *AAV$_9$-SST-Flp* (BC-0429, vector backbone from Addgene: 22913),
517 *AAV$_9$-Ef1α-fDIO-ChR2-mCherry* (BC-0113), *AAV$_9$-Ef1α-fDIO-mCherry* (BC-0193)
518 and *AAV$_9$-Ef1α-fDIO-hM3Dq-mCherry* (BC-0495) were purchased from Brain Case
519 Co., Ltd. (Shenzhen, China).

520 **Stereotaxic surgery**

521 Mice were anesthetized with 2% isoflurane and placed in a stereotaxic instrument
522 (RWD Life Science, Shenzhen, China). Microinjections were performed using 33-
523 gauge needles connected to a 10 μl microsyringe (Hamilton, Bonaduz, Switzerland),
524 which were under the control of a UMP3 ultra micropump (World Precision Instruments,
525 Florida, USA). The coordinates relative to bregma were listed as follows: anterior-
526 posterior (AP) - 1.9 mm; medial-lateral (ML) ± 1.1 mm; dorsal-ventral (DV) - 2.1 mm
527 for DG and AP - 4.7 mm; ML ± 3.2 mm; DV - 4.5 mm for MEC. The needle was slowly
528 lowered to the target site and remained for at least 3 min after injection. The injection
529 volume per site was 0.3 μl in DG and 0.4 μl in MEC. The final titer of all the AAVs
530 used for infections were at least 1×10^{12} V.G./ml except for *AAV-SST-Flp, AAV-PV-Flp,*
531 *AAV-VGAT2-Flp, AAV-Fos-RAM-d2tTA-TRE-Cre* and *AAV-Npas4-RAM-d2tTA-TRE-*
532 *Cre,* which were 1:1000 diluted. For rabies infections, the final titer used was 1×10^{8}
533 IFU/ml. After surgery, all mice were given at least 3 weeks to recover before behavioral
534 experiments or electrophysiological recordings, and the efficiency of virus infection
535 was verified by immunostaining. Only the mice with virus infection in correct places
536 were chosen for further analysis.

537 **Engram labeling**

538 To label engram cells, *Fos-RAM-d2tTA-TRE (F-RAM)* and *Npas4-RAM-d2tTA-TRE (N-*
539 *RAM)* systems, which gene expression was under the control of the tetracycline
540 responsive element (TRE), were used respectively through AAVs infusion. All mice
541 were kept on doxycycline (Dox, Huamaike Bio, 360304) containing food (40 mg/kg)
542 one day before virus injection. 48 hr (day -2) before engram labeling, mice were fed
543 with regular food instead of Dox diet. Then contextual fear conditioning or novel
544 context exposure (context N) was performed on day 0 to label Fos^+ or $Npas4^+$ engram
545 cells in DG, after labeling, mice were put on Dox containing food again immediately.
546 Mice were given at least 3 days to allow sufficient protein expression before subsequent
547 experiments.

548 **Rabies input tracing**

549 To study the respective monosynaptic inputs of Fos^+ and $Npas4^+$ ensembles in DG,
550 Rabies trans-synaptic tracing experiment was performed. Mice were infected with
551 AAV_9*-Fos-RAM-d2tTA-TRE-Cre* or AAV_9*-Npas4-RAM-d2tTA-TRE-Cre,* AAV helper
552 (AAV_8*-Ef1α-DIO-TVA-H2B-EGFP* and AAV_8*-Ef1α-DIO-RVG*). On day 3 after engram
553 labeling, Rabies virus (*RV-ENVA-ΔG-dsRed*) was injected into DG at the same
554 coordinates, then mice were housed in the BSL2 facility for 1 week to allow rabies
555 spread and dsRed expression before perfusion (day 10). For rabies tracing analysis,
556 consecutive brain slices from AP + 2.8 mm to AP - 5.0 mm (40 μm thickness) selected
557 from every fifth slice were collected. $DsRed^+$ cells were manually counted by an
558 experimenter who was blind to the experimental condition. The percentage of rabies-
559 labelled inputs was calculated as follows, $dsRed^+$ cells in each brain region / total

560 dsRed^{+} cells per mouse.

561 **Contextual fear conditioning (CFC)**

562 Before CFC was performed, mice were handled daily in a holding room for 3 days. For
563 experiments with Dox-dependent ensembles labeling, on the third handling day, the
564 Dox diet was replaced with regular food (off-Dox) and CFC assay was typically carried
565 out 48 hours after the last handling session. CFC was performed in the conditioning
566 chamber (Med-Associates, St. Albans, VT, USA) and the procedure was composed of
567 conditioning and test sessions.

568 On the conditioning day (day 0), mice were firstly transported into the holding room
569 and allowed to habituate for at least 30 minutes, then transported into the behavioral
570 room and placed into context A, a square plexiglass observational chamber with
571 stainless steel bars connected to a shock generator on the floor for conditioning. Two
572 individual conditioning protocols were used in our study, for mice that conditioned to
573 the 360 s protocol, three foot shocks (0.5 mA, 1 s each) at 180 s, 240 s and 300 s were
574 given and mice were taken out 60 s after termination of the third foot shock, for mice
575 that conditioned to the180 s protocol, one single foot shock (0.3 mA, 1 s) at 120 s was
576 given and mice were taken out 60 s after termination of the foot shock.

577 The test session was carried out on day 3. Mice were put back into fear context A for
578 180 s, and were placed into a non-fear context (context C, a triangular chamber with
579 white, smooth plastic floor and black cover) for 180 s 6 hr later. For
580 immunohistochemistry, mice were tested for memory expression in only one context,
581 either context A or C, and sacrificed 1 hr later.

582 The freezing percentage was automatically analyzed by software (Med-Associates)
583 with freezing defined as absence of movement for at least 1 s. The discrimination index
584 (DI) was calculated as follows, (the freezing percentage in context A - the freezing
585 percentage in context C) / (the freezing percentage in context A + the freezing
586 percentage in context C).

587 **Open field test (OFT)**

588 Spontaneous locomotor activity was carried out as we previously reported[42], in short,
589 mice were placed in the center of an open arena (40 × 40 cm^2) at the beginning of the
590 test, and were allowed to freely explore the arena for 20 min. Distance travelled in the
591 arena and time in center zone were quantified using a TopScan automated detection
592 system (CleverSys, Reston, VA, USA).

593 **O-maze test**

594 The O-maze was 70 cm in diameter and 70 cm high off the ground, and consisted of
595 two open arms (7 cm wide) without walls, two closed arms that were enclosed by
596 vertical walls. Mice were gently placed into the open arms, and their behavior was
597 recorded for 6 min via a TopScan automated detection system (CleverSys, Reston, VA,
598 USA) located above the maze.

599 **Tail suspension test (TST)**

600 Mice were suspended 20 cm above a solid surface by the use of adhesive tape applied
601 to the tail, and their behavior was recorded for 6 min. Immobility time was defined as
602 absence of struggling for at least 1 s and latency to immobility was defined as the time
603 from the beginning of TST to mice's first absence of struggling for at least 1 s, which

604 were manually analyzed by an experimenter who was blind to the experimental
605 condition.

606 **Drug injections**

607 Clozapine N-oxide (CNO, Sigma, C0832) was dissolved in saline, which was
608 intraperitoneal injected (i.p.) at a concentration of 1 mg/kg 30 min before memory
609 retrieval. The KCNQ2/3 activator, retigabine (Supelco, 90221) was diluted in 5%
610 DMSO (Sigma, 276855) and administered i.p. at 1 mg/kg 30 min before memory
611 retrieval with 5% DMSO as control. 4-Hydroxytamoxifen (4-OHT, Sigma, H6278) was
612 dissolved in ethanol at 20 mg/ml and stored at -20℃. The ethanol was evaporated at
613 95℃ and corn oil (Thermo Fisher, C40543) was added to give a final concentration of
614 10 mg/ml, which was i.p. injected 2 hr before memory conditioning with corn oil as
615 control.

616 **Whole-cell patch-clamp recording in brain slices**

617 Mice were subjected to electrophysiology on day 3 following CFC. Living acute brain
618 slices (300 μm) preparation for analyzing engram synaptic connections and engram
619 intrinsic excitability were performed as previously described[43] only with minor
620 modifications. Briefly, mice's brains were cut on a vibratome (Thermo Scientific, MA,
621 USA) in carbogenated (95% O_2, 5% CO_2) ice-cold cutting solution containing (in mM):
622 93 NMDG, 2.5 KCl, 1.25 NaH_2PO_4, 30 $NaHCO_3$, 20 HEPES, 25 glucose, 2 thiourea, 5
623 Na-ascorbate, 3 Na-pyruvate, 0.5 $CaCl_2$ and 10 $MgCl_2$, 300-310 mOsm, pH adjusted to
624 7.3 with HCl. After initial recovery at 32 °C for 10 min, slices were transferred to
625 carbogenated HEPES holding ACSF (in mM: 92 NaCl, 2.5 KCl, 1.25 NaH_2PO_4, 30

626 $NaHCO_3$, 20 HEPES, 25 glucose, 2 thiourea, 5 Na-ascorbate, 3 Na-pyruvate, 2 $CaCl_2$
627 and 2 $MgCl_2$, 300-310 mOsm, pH 7.4) and incubated for over 45 min before recording.
628 Whole-cell patch-clamp recordings were performed in carbogenated recording ACSF
629 (in mM: 119 NaCl, 2.5 KCl, 1.25 NaH_2PO_4, 24 $NaHCO_3$, 12.5 glucose, 2 $CaCl_2$ and 2
630 $MgCl_2$ (300-310 mOsm, pH 7.3-7.4) at a rate of 1.5 mL / min (30~32°C) with an EPC-
631 10 amplifier and Pulse v8.78 software (HEKA Elektronik, Lambrecht/Pfalz, Germany).
632 Recording neurons were identified visually by location, morphology, size and
633 fluorescence and recordings were performed using borosilicate glass pipettes (5-7 MΩ
634 tip resistance).
635 To record A/N ratios, neurons were voltage-clamped at -70 mV to record AMPAR
636 mediated EPSCs and at +40 mV to record dual-component EPSCs containing NMDA
637 receptor (NMDAR) EPSCs. To calculate the A/N ratios, the peak current of the AMPA
638 EPSC at -70 mV was compared with the value of the NMDA EPSC after stimulation
639 start time 50 ms at +40 mV. Intracellular solution used was (in mM): 127.5 cesium
640 methanesulfonate, 7.5 CsCl, 10 HEPES, 2.5 $MgCl_2$, 4 Mg-ATP, 0.4 Na_3-GTP, 10
641 sodium phosphocreatine, 0.6 EGTA (290-300 mOsm, pH 7.2).
642 To record light-evoked EPSCs (oEPSC), A TTL-driven light-emitting diode (Lumen
643 Dynamics) was used to generate photostimulation consisting of a single wide-field blue
644 flash (470 nm, 1 ms duration) for photostimulation of ChR2-expressing terminals. The
645 laser intensity was measured at the focal plane of the slice when delivered through the
646 40× water-immersion objective lens (Nikon, Japan). Slices containing MEC ChR2-
647 expressing terminals were chosen for oEPSC recording in the presence of 1 μM

648 Tetrodotoxin (TTX, Tocris, 1078), 100 μM 4-aminopyridine (4-AP, Sigma, 275875)
649 and 100 μM picrotoxin (PTX, Tocris, 1128), neurons were voltage-clamped at -70 mV
650 and the stimulus intensity was 0.1 mW at 470 nm. To record paired-pulse ratio (PPR)
651 and AMPA/NMDA (A/N) EPSC ratio, DG slices containing ChR2-expressing neurons
652 were chosen to perform patch-clamp recordings in the presence of 100 μM PTX and
653 the stimulus intensity was 0.1 mW at 470 nm. The AMPA receptor (AMPAR) mediated
654 EPSCs were evoked by paired photostimulation of 50 ms interval for 10 consecutive
655 traces, and PPR was determined as the peak amplitude ratio of the second to the first
656 EPSC. To record light-evoked IPSCs (oIPSC) and PPR, neurons were clamped at +10
657 mV in the presence of 1 μM TTX, 100 μM 4-AP, 20 μM CNQX (Sigma, C127) and 50
658 μM D-AP5 (Tocris, 0106) and the stimulus duration and intensity was 1 ms, 0.2 mW at
659 470 nm. The recording protocols and intracellular solution used were the same as above.
660 To record Action Potentials (AP), current-clamp was used and membrane potentials
661 were measured in response to intracellular injection of step currents (1000 ms duration,
662 magnitudes ranging from - 150 to 250 pA in steps of 10 pA) with the addition of 20 μM
663 CNQX, 50 μM D-AP5 and 100 μM PTX into ACSF. Intracellular solution used was (in
664 mM): 135 potassium-gluconate, 4 KCl, 2 NaCl, 10 HEPES, 4 EGTA, 4 Mg-ATP, 0.3
665 Na3-GTP, 10 sodium phosphocreatine (280-290 mOsm, pH 7.3).
666 To record and isolate M-current (I_M), intracellular solution used was the same as above,
667 0.2 mM $CdCl_2$ (Sigma, 202908), 1 μM TTX, 10 μM ZD7288 (Tocris, 1000), and 4 mM
668 4-AP to block voltage-dependent Cav, Nav, HCN and Kv1 channels, 20 μM CNQX, 50
669 μM D-AP5 and 100 μM picrotoxin to block synaptic activity were added into ACSF.

670 To isolate M-current, the following protocol the same as previously reported[44] with
671 minor modifications was applied to the recording cells: (1) a 1 s step from the holding
672 potential (-70 mV) to -10 mV was applied to activate I_M while inactivating most other
673 voltage-gated currents, (2) a 1 s step from -60 mV to -10 mV with 10 mV increments
674 to elicit I_M tail current, and (3) a 1 s step to -10 mV, before returning to -70 mV.
675 The signals were acquired at 10 kHz and filtered at 2 kHz. The series resistance was <
676 30 MΩ. Data were analyzed with Mini Analysis Program (Synaptosoft, Fort Lee, NJ,
677 USA) or pCLAMP10.7 (Molecular Devices, San Jose, CA, USA) by an experimenter
678 who was blind to the experimental condition.

679 **Ribosome-Associated Messenger RNA Purification/ RiboTag**

680 DG from mice injected *AAV9-F/N-RAM-Cre* and *AAV9-Flex-NBL10,* Cre-dependent
681 expression of N terminus of ribosomal subunit protein Rpl10a (NBL10)[45] following
682 fear conditioning (Day 3) was quickly isolated and used for enrichment of ribosome-
683 associated transcripts as described previously[18]. The brain tissue (DG) was
684 homogenized in supplemented hybridization buffer (HB-S) containing dithiothreitol
685 (DTT, Sigma, D9760), cycloheximide (CHX, Cayman, 14126), heparin (Tocris, 2812),
686 protease inhibitors (Roche, 04693116001), and RNase inhibitor (Vazyme, R301). The
687 supernatant was incubated with anti-hemagglutinin (HA) antibody (Sigma, H6908) and
688 Dynabeads Protein G (Invitrogen, 10003D) for 12 hours. Purified messenger RNA
689 (mRNA) was eluted from the Dynabeads using TRIzol™ LS (Invitrogen, 10296010).
690 An Agilent RNA 6000 Pico Kit (Agilent, 5067-1513) and an Agilent 2100 bioanalyzer
691 were used to evaluate the quality of purified mRNA. Purified mRNA samples with RNA

692 integrity number < 7 were discarded.

693 **Sequence Processing and Data Analysis**

694 The library was prepared with VAHTSTM mRNA-seq V3 Library Prep Kit for Illumina
695 (Vazyme, NR611) and sequenced on a HiSeq 4000 (Illumina) by Novogene Technology
696 Co., Ltd (Beijing, China). Raw reads were cleaned with FASTX-toolkit to remove
697 adapter contamination and low-quality reads (quality score < 28). The clipped reads
698 were aligned to mouse reference sequence (GRCm38/mm10) using HISAT2[46].
699 Cuffdiff-generated FPKM count matrix was used for subsequent analysis. Significance
700 was drawn with ANOVA and clustered using Shannon entropy-based method[47]. Genes
701 with more than one and half fold expression changes, and were significantly different
702 ($P < 0.05$) were selected for further analysis.

703 **Single molecule fluorescent in situ hybridization (smFISH)**

704 Fixed-frozen brain tissues were sliced into 10 μm coronal sections and baked at 60ºC
705 for 30 min. Then slices were incubated with hydrogen peroxide (H_2O_2) for 10 min at
706 room temperature (RT), targets retrieval and protease III incubation were performed
707 using RNAscope® 2.5 Universal Pretreatment Reagents (Advanced Cell Diagnostics,
708 322000, 322381). SmFISH probes for all genes examined: *Nptx1* (505421), *Nptx2*
709 (316901), *Fos* (316921), *Npas4* (423431), *Sirt1* (418341) and *Atg7* (561261) were
710 hybridized for 2 hr. After Hybridization, RNAscope® Multiplex Fluorescent Detection
711 Kit v2 (Advanced Cell Diagnostics, 323110) were used to amplify signals. Images were
712 acquired by using the Nikon A1 confocal microscope (Tokyo, Japan). Regions of
713 interest (ROI) were circled and the intensity within the regions was analyzed by Image-

714 Pro Plus 6.0 (Media Cybernetics, Rockville, MD, USA). For cell counting analysis,
715 consecutive brain slices from AP – 1.2 mm to AP – 2.0 mm (10 μm thickness) selected
716 from every tenth slice, 8 slices per mouse were collected, number of mice were included
717 in the statistical table.

718 **Immunohistochemistry (IHC)**

719 Mice were perfused transcardially with ice cold saline followed by 4%
720 paraformaldehyde (PFA, dissolved in 0.1 M PBS). The brains were removed and fixed
721 in 4% PFA overnight. Then the brains were subjected to dehydrate in 30% sucrose
722 solutions at 4°C for 72 hr before being sliced into 30 or 40 μm coronal sections (selected
723 from every fifth slice). Slices were incubated with primary antibodies in blocking
724 solution containing 0.3% Triton X-100 overnight at 4ºC. Slices were washed with 0.1
725 M PBS, and then incubated with secondary antibody at RT for 1.5 hr. After being
726 washed in PBS, slices were mounted in anti-quenching mounting medium (Southern
727 Biotech, 0100). Primary antibodies used were: anti-NPTX1 (1:400, Alomone Labs,
728 ANR-191), anti-NPTX2 (1:500, Proteintech, 10889-1-AP), anti-Fos (1:500, Synaptic
729 Systems, 226017), anti-Parvalbumin (PV, 1:100, Thermo Fisher, PA1-933), anti-PV
730 (1:500, Oasis, OB-PGP005-01), anti-GluA4 (1:500, Merck, AB1508), anti-
731 Somatostatin (SST, 1:200, Oasis, OB-PRB111-01), anti-Choline Acetyltransferase
732 (ChAT, 1:100, Merck, AB143), anti-Glutamate (1:500, Merck, AB133), anti-GAD67
733 (1:500, Merck, MAB5406), anti-cholecystokinin (CCK, 1:1000, Merck, C2581) and
734 anti-KCNQ2 (1:100, Alomone Labs, APC-050). Secondary antibodies used were: goat
735 anti-rat 488 (1:1000, Jackson Immuno Research, 112-545-167), goat anti-rabbit 488

736 (1:1000, Jackson Immuno Research, 111-545-144), donkey anti-guinea pig 488 (1:1000,
737 Jackson Immuno Research, 706-545-148), goat anti-rabbit Cy3 (1:1000, Jackson
738 Immuno Research, 111-165-144), donkey anti-rat Cy3 (1:1000, Jackson Immuno
739 Research, 712-165-153) and donkey anti-rat 647 (1:500, Jackson Immuno Research,
740 712-605-150). Kv7.2 and GluA4 membrane expression analysis were adapted from one
741 of the latest researches from our lab[48]. Images were acquired using a Nikon-A1 confocal
742 microscope (Tokyo, Japan) with a 20× objective lens or a 60× objective oil lens. Data
743 were analyzed blindly to the group using Image-Pro Plus 6.0 and ImageJ (Fiji). For cell
744 counting analysis, consecutive brain slices from AP – 1.2 mm to AP – 2.0 mm (40 μm
745 thickness) selected from every fifth slice, 4 slices per mouse were collected, number of
746 mice were included in the statistical table.

747 **Reverse transcription-quantitative PCR (RT-qPCR)**

748 Reverse transcription was completed using HiScript II 1st Strand cDNA Synthesis Kit
749 (Vazyme, R212). The cDNA was subjected to qPCR using ChamQ Universal SYBR
750 qPCR Master Mix (Vazyme, Q711) and Eppendorf Mastercycler PCR System. The
751 primers for qPCR were as follows: 5' - ACCTCCCTACACCAACGGAT - 3' and 5' -
752 GGCAGGCTCTTCTTCACCTT - 3' for *Nptx1*, 5' - GCCAAGGTGAAGAAGAGCCT
753 - 3' and 5' - AGCATAAGAGAAGGGTGTGCC - 3' for *Nptx1* of exon 3, 5' -
754 GACTTCCGAGAGGTGCTCCA - 3' and 5' - GGTGAGCCGAGGTCTCATTA - 3' for
755 *Nptx2* of exon 2, 5' - TGGCCTTCCGTGTTCCTAC - 3' and 5' -
756 GAGTTGCTGTTGAAGTCGCA - 3' for *Gapdh*, which were synthesized by Azenta
757 US, Inc.. The mRNA expression of *Nptx1* and *Nptx2* was normalized to the internal

control *Gapdh*.

Co-immunoprecipitation (Co-IP) and Western blotting

The DG tissues of adult C57BL/6J male mice were rapidly extracted and homogenized in radio immunoprecipitation assay (RIPA) buffer containing protease and phosphatase inhibitors for 30 min. The protein lysate concentration was determined using bicinchoninic acid kit. Protein samples were incubated with 3 μg anti-NPTX1 (Santa Cruz Biotechnology, sc-374199) or anti-IgG (Cell Signaling Technology, 5415S) for 4 h at 4ºC. Pierce Protein A/G magnetic beads (88803, Thermo Scientific) were added to each sample and the mixture was rotated at 4°C overnight. The attached protein lysis was then eluted and used for further protein blotting assay. Before Western blotting assay, 50 μg protein samples were boiled for 6 min at 85ºC, and were separated by SDS-polyacrylamide gel electrophoresis (PAGE) under 120 V for 1.5 h. Proteins were then transferred to the polyvinylidene fluoride (PVDF) membrane at 100 mV for 100 min. The membrane was firstly washed with Tris-buffered saline with Tween 20 (TBST), followed by blocking in 5% skimmed milk for 2 hours. The membrane was then incubated with the following primary antibodies anti-NPTX1 (1:100, Santa Cruz Biotechnology, sc-374199) and anti-KCNQ2 (1:500, Abcam, ab22897) at 4°C overnight. On the next day, the membrane was washed with TBST and incubated with IRDye 700DX- or 800DX-conjugated anti-rabbit or anti-mouse IgG (1:50000, Rockland Immunochemicals Inc.) for 2 h at room temperature. Protein bands were visualized using Odyssey (LI-COR Biosciences). The immunoblots were analyzed with Image J.

Statistics

All data were presented as mean ± SEM. Sample sizes were based on our previous research[18,42,49]. Statistical analyses were performed by SPSS 20.0 software (IBM, Armonk, NY, USA) or R software (version 4.1.2). The normality test of the data sets was performed by the Shapiro-Wilk test or the Kolmogorov-Smirnov test if n > 50, homogeneity of variance test of the data sets was performed by the Levene's test. Two-tailed unpaired *t* test was used for comparing two independent groups. Multiple group comparisons were assessed using One-way analysis of variance (ANOVA), Two-way ANOVA or Two-way repeated measures (RM) ANOVA, followed by the Bonferroni's post-hoc test when significant main effects or interactions were detected. Mann-Whitney *U* test or Kruskal-Wallis H test was used when normality was violated. For human sample analysis, all CSF protein levels were Z-transformed. The linear mixed-effects (LME) models with random slopes and intercepts were employed to examine the associations of CSF NPTX1 and NPTX2 with longitudinal changes in cognitive scores. Considering the small sample size with follow-up over 50 months, we deleted these subjects from the analysis. LME models included the interaction between time and CSF protein as the predictor of changes in specific cognitive outcomes. Age, sex, years of education, *APOE* ε4 alleles and baseline diagnosis were included as covariates. All cognitive variables in the LME models were Z-transformed to facilitate comparisons between modalities. Bonferroni's corrections were applied to assess statistical significance.* $P < 0.05$, ** $P < 0.01$, and *** $P < 0.001$.

References

1 Josselyn, S. A. & Tonegawa, S. Memory engrams: Recalling the past and imagining the future. *Science* **367** (2020).

2 Tonegawa, S., Morrissey, M. D. & Kitamura, T. The role of engram cells in the systems consolidation of memory. *Nature Reviews Neuroscience* **19**, 485-498 (2018).

3 Castello-Waldow, T. P. *et al.* Hippocampal neurons with stable excitatory connectivity become part of neuronal representations. *Plos Biol* **18** (2020).

4 Luo, L. & Craik, F. I. Aging and memory: a cognitive approach. *Can J Psychiatry* **53**, 346-353 (2008).

5 Fan, X., Wheatley, E. G. & Villeda, S. A. Mechanisms of Hippocampal Aging and the Potential for Rejuvenation. *Annu Rev Neurosci* **40**, 251-272 (2017).

6 Sudhof, T. C. Towards an Understanding of Synapse Formation. *Neuron* **100**, 276-293 (2018).

7 Gomez de San Jose, N. *et al.* Neuronal pentraxins as biomarkers of synaptic activity: from physiological functions to pathological changes in neurodegeneration. *J Neural Transm (Vienna)* **129**, 207-230 (2022).

8 Cho, R. W. *et al.* mGluR1/5-dependent long-term depression requires the regulated ectodomain cleavage of neuronal pentraxin NPR by TACE. *Neuron* **57**, 858-871 (2008).

9 Xu, D. *et al.* Narp and NP1 form heterocomplexes that function in developmental and activity-dependent synaptic plasticity. *Neuron* **39**, 513-528 (2003).

10 Abad, M. A., Enguita, M., DeGregorio-Rocasolano, N., Ferrer, I. & Trullas, R. Neuronal pentraxin 1 contributes to the neuronal damage evoked by amyloid-beta and is overexpressed in dystrophic neurites in Alzheimer's brain. *J Neurosci* **26**, 12735-12747 (2006).

11 Figueiro-Silva, J. *et al.* Neuronal pentraxin 1 negatively regulates excitatory synapse density and synaptic plasticity. *J Neurosci* **35**, 5504-5521 (2015).

12 Chang, M. C. *et al.* Narp regulates homeostatic scaling of excitatory synapses on parvalbumin-expressing interneurons. *Nat Neurosci* **13**, 1090-1097 (2010).

13 Gu, Y. *et al.* Obligatory Role for the Immediate Early Gene NARP in Critical Period Plasticity. *Neuron* **79**, 335-346 (2013).

14 Xiao, M. F. *et al.* A biomarker-authenticated model of schizophrenia implicating NPTX2 loss of function. *Sci Adv* **7**, eabf6935 (2021).

15 Mravinacová, S. *et al.* CSF protein ratios with enhanced potential to reflect Alzheimer's disease pathology and neurodegeneration. *Mol Neurodegener* **19** (2024).

16 Soldan, A. *et al.* NPTX2 in Cerebrospinal Fluid Predicts the Progression From Normal Cognition to Mild Cognitive Impairment. *Ann Neurol* **94**, 620-631 (2023).

17 Sun, X. *et al.* Functionally Distinct Neuronal Ensembles within the Memory Engram. *Cell* **181**, 410-423 e417 (2020).

18 Wang, Z. *et al.* Retrieval-Driven Hippocampal NPTX2 Plasticity Facilitates the Extinction of Cocaine-Associated Context Memory. *Biol Psychiatry* **87**, 979-991 (2020).

19 Mariga, A. *et al.* Definition of a Bidirectional Activity-Dependent Pathway Involving BDNF and Narp. *Cell Rep* **13**, 1747-1756 (2015).

20 Delmas, P. & Brown, D. A. Pathways modulating neural KCNQ/M (Kv7) potassium channels.

Nat Rev Neurosci **6**, 850-862 (2005).

21 Li, S. B. *et al.* Hyperexcitable arousal circuits drive sleep instability during aging. *Science* **375**, eabh3021 (2022).

22 Topolnik, L. & Tamboli, S. The role of inhibitory circuits in hippocampal memory processing. *Nat Rev Neurosci* **23**, 476-492 (2022).

23 Royer, S. *et al.* Control of timing, rate and bursts of hippocampal place cells by dendritic and somatic inhibition. *Nat Neurosci* **15**, 769-775 (2012).

24 Cummings, D. M. *et al.* Neuronal and Peripheral Pentraxins Modify Glutamate Release and may Interact in Blood-Brain Barrier Failure. *Cereb Cortex* **27**, 3437-3448 (2017).

25 Pelkey, K. A. *et al.* Pentraxins Coordinate Excitatory Synapse Maturation and Circuit Integration of Parvalbumin Interneurons. *Neuron* **90**, 661 (2016).

26 Blackburn-Munro, G., Dalby-Brown, W., Mirza, N. R., Mikkelsen, J. D. & Blackburn-Munro, R. E. Retigabine: chemical synthesis to clinical application. *CNS Drug Rev* **11**, 1-20 (2005).

27 Bieri, G., Schroer, A. B. & Villeda, S. A. Blood-to-brain communication in aging and rejuvenation. *Nat Neurosci* **26**, 379-393 (2023).

28 Regev, N. *et al.* Selective interaction of syntaxin 1A with KCNQ2: possible implications for specific modulation of presynaptic activity. *PLoS One* **4**, e6586 (2009).

29 Luna, V. M. *et al.* Adult-born hippocampal neurons bidirectionally modulate entorhinal inputs into the dentate gyrus. *Science* **364**, 578-583 (2019).

30 Qin, H. *et al.* A Visual-Cue-Dependent Memory Circuit for Place Navigation. *Neuron* **99**, 47-55 e44 (2018).

31 Bartos, M. & Elgueta, C. Functional characteristics of parvalbumin- and cholecystokinin-expressing basket cells. *J Physiol* **590**, 669-681 (2012).

32 Klausberger, T. *et al.* Complementary roles of cholecystokinin- and parvalbumin-expressing GABAergic neurons in hippocampal network oscillations. *J Neurosci* **25**, 9782-9793 (2005).

33 Sun, X. & Lin, Y. Npas4: Linking Neuronal Activity to Memory. *Trends Neurosci* **39**, 264-275 (2016).

34 Spiegel, I. *et al.* Npas4 regulates excitatory-inhibitory balance within neural circuits through cell-type-specific gene programs. *Cell* **157**, 1216-1229 (2014).

35 Pollina, E. A. *et al.* A NPAS4-NuA4 complex couples synaptic activity to DNA repair. *Nature* **614**, 732-741 (2023).

36 Bloodgood, B. L., Sharma, N., Browne, H. A., Trepman, A. Z. & Greenberg, M. E. The activity-dependent transcription factor NPAS4 regulates domain-specific inhibition. *Nature* **503**, 121-125 (2013).

37 Yap, E. L. *et al.* Bidirectional perisomatic inhibitory plasticity of a Fos neuronal network. *Nature* **590**, 115-121 (2021).

38 Ramsaran, A. I. *et al.* A shift in the mechanisms controlling hippocampal engram formation during brain maturation. *Science* **380**, 543-551 (2023).

39 Gold, L. *et al.* Aptamer-Based Multiplexed Proteomic Technology for Biomarker Discovery. *Plos One* **5** (2010).

40 Candia, J. *et al.* Assessment of Variability in the SOMAscan Assay. *Sci Rep-Uk* **7** (2017).

41 Chen, P. D. *et al.* Four Distinct Subtypes of Alzheimer?s Disease Based on Resting-State Connectivity Biomarkers. *Biol Psychiat* **93**, 759-769 (2023).

42 Jin, T. *et al.* Dorsal hippocampus- and ACC-projecting medial septum neurons differentially contribute to the recollection of episodic-like memory. *FASEB J* **34**, 11741-11753 (2020).

43 Ting, J. T., Daigle, T. L., Chen, Q. & Feng, G. Acute brain slice methods for adult and aging animals: application of targeted patch clamp analysis and optogenetics. *Methods Mol Biol* **1183**, 221-242 (2014).

44 Lopez, J. P. *et al.* Ketamine exerts its sustained antidepressant effects via cell-type-specific regulation of Kcnq2. *Neuron* **110**, 2283-2298 e2289 (2022).

45 Ekstrand, M. I. *et al.* Molecular profiling of neurons based on connectivity. *Cell* **157**, 1230-1242 (2014).

46 Kim, D., Paggi, J. M., Park, C., Bennett, C. & Salzberg, S. L. Graph-based genome alignment and genotyping with HISAT2 and HISAT-genotype. *Nat Biotechnol* **37**, 907-915 (2019).

47 Ghosh, S. & Chan, C. K. Analysis of RNA-Seq Data Using TopHat and Cufflinks. *Methods Mol Biol* **1374**, 339-361 (2016).

48 He, G. *et al.* Persistent increase of accumbens cocaine ensemble excitability induced by IRK downregulation after withdrawal mediates the incubation of cocaine craving. *Mol Psychiatry* **28**, 448-462 (2023).

49 Zhou, Y. *et al.* A ventral CA1 to nucleus accumbens core engram circuit mediates conditioned place preference for cocaine. *Nat Neurosci* **22**, 1986-1999 (2019).

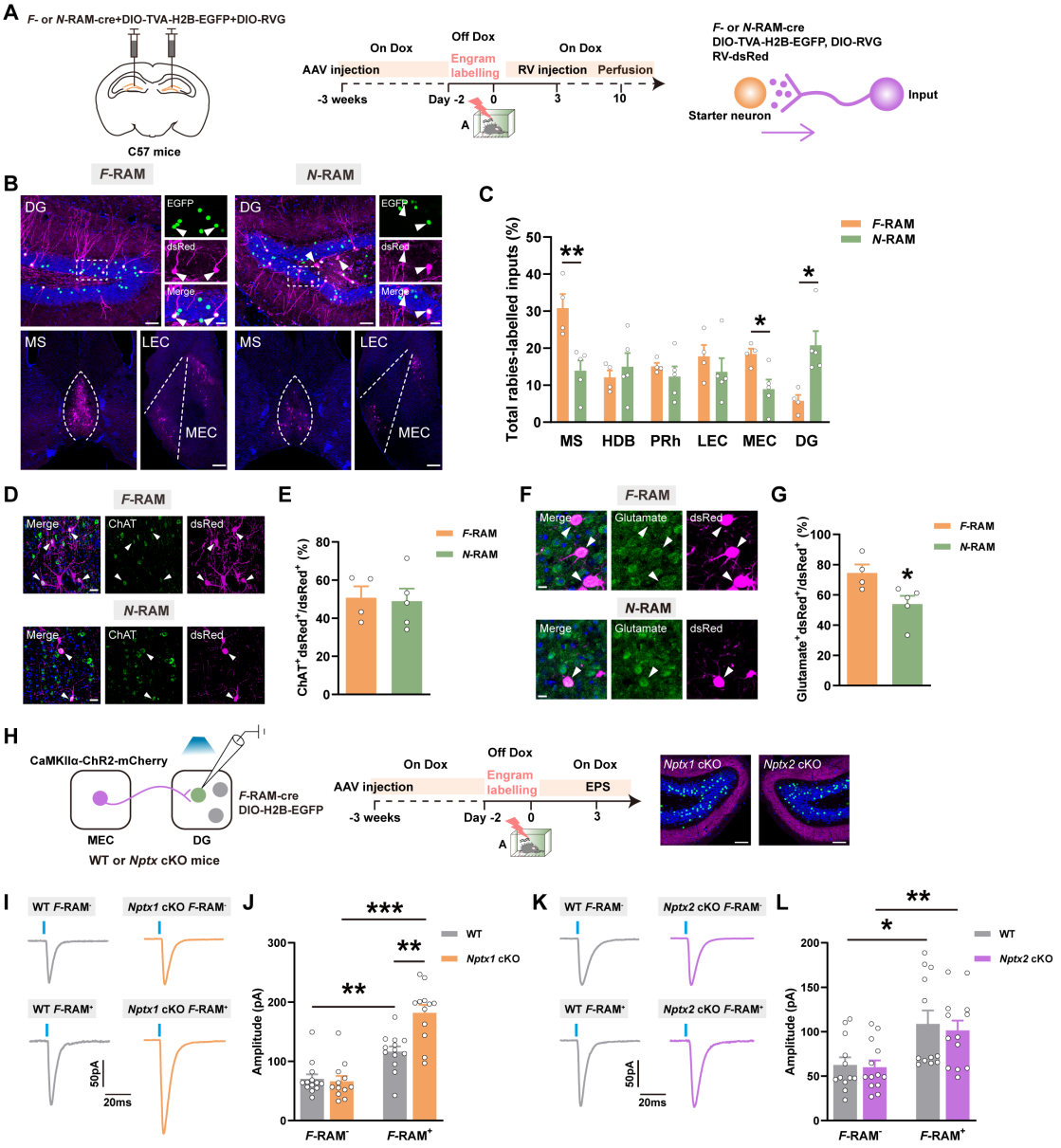
A
F- or N-RAM-cre+DIO-TVA-H2B-EGFP+DIO-RVG
C57 mice
On Dox
Off Dox
On Dox
AAV injection
Engram labelling
RV injection
Perfusion
-3 weeks
Day -2
0
3
10
F- or N-RAM-cre
DIO-TVA-H2B-EGFP, DIO-RVG
RV-dsRed
Starter neuron
Input
B
F-RAM
N-RAM
DG
EGFP
dsRed
Merge
MS
LEC
MEC
C
Total rabies-labelled inputs (%)
F-RAM
N-RAM
MS
HDB
PRh
LEC
MEC
DG
D
ChAT
E
ChAT+dsRed+/dsRed+ (%)
F
Glutamate
G
Glutamate+dsRed+/dsRed+ (%)
H
CaMKIIα-ChR2-mCherry
F-RAM-cre
DIO-H2B-EGFP
MEC
DG
WT or Nptx cKO mice
EPS
Nptx1 cKO
Nptx2 cKO
I
WT F-RAM-
Nptx1 cKO F-RAM-
WT F-RAM+
Nptx1 cKO F-RAM+
50pA
20ms
J
Amplitude (pA)
WT
Nptx1 cKO
F-RAM-
F-RAM+
K
Nptx2 cKO F-RAM-
Nptx2 cKO F-RAM+
L
Nptx2 cKO

910 **Figure 1. Rabies virus tracing of the upstream inputs to DG *F*- and *N*-RAM**
911 **neuronal ensembles and the effects of *Nptxs* depletion on response to MEC**
912 **excitatory inputs.** (A) Diagram of virus injection and experimental scheme to trace
913 upstream inputs of DG *F*-RAM and *N*-RAM ensembles. (B) Representative confocal
914 images of DG starter neurons in *F*-RAM, *N*-RAM ensembles and their respective
915 upstream inputs. Green: *F*-RAM or *N*-RAM engram cells, EGFP, Purple: dsRed, Blue:
916 DAPI. White arrows indicate the starter neurons and DG local inputs. Scale bar: top
917 left, 50 μm, top right, 10 μm, bottom, 100 μm. (C) The percentages of total inputs from
918 each upstream site relative to total quantified inputs. (D) Representative confocal
919 images of upstream MS $dsRed^+$ cells immunostaining with ChAT. Green: ChAT, Purple:
920 dsRed, Blue: DAPI. White arrows indicate the colocalized cells. Scale bar: 10 μm. (E)
921 The percentages of colocalized cells in MS total $dsRed^+$ cells. (F) Representative
922 confocal images of upstream MEC $dsRed^+$ cells immunostaining with glutamate. Green:
923 glutamate, Purple: dsRed, Blue: DAPI. White arrows indicate the colocalized cells.
924 Scale bar: 5 μm. (G) The percentages of colocalized cells in MEC total $dsRed^+$ cells.
925 (H) Diagram of AAV injection, experimental scheme and representative expression of
926 ChR2 in MEC projection neurons and DG engram cells. Green: *F*-RAM engram cells
927 of *Nptx1* and *Nptx2* cKO mice, EGFP, Purple: MEC projections, mCherry, Blue: DAPI.
928 Scale bar: 50 μm. (I, K) Representative traces of oEPSC recorded from WT and *Nptxs*
929 cKO mice. (J) The quantification of oEPSC amplitudes recorded from WT and *Nptx1*
930 cKO mice. (L) The quantification of oEPSC amplitudes recorded from WT and *Nptx2*
931 cKO mice. Data are presented as mean ± S.E.M; $*P < 0.05$, $**P < 0.01$, $***P < 0.001$.
932

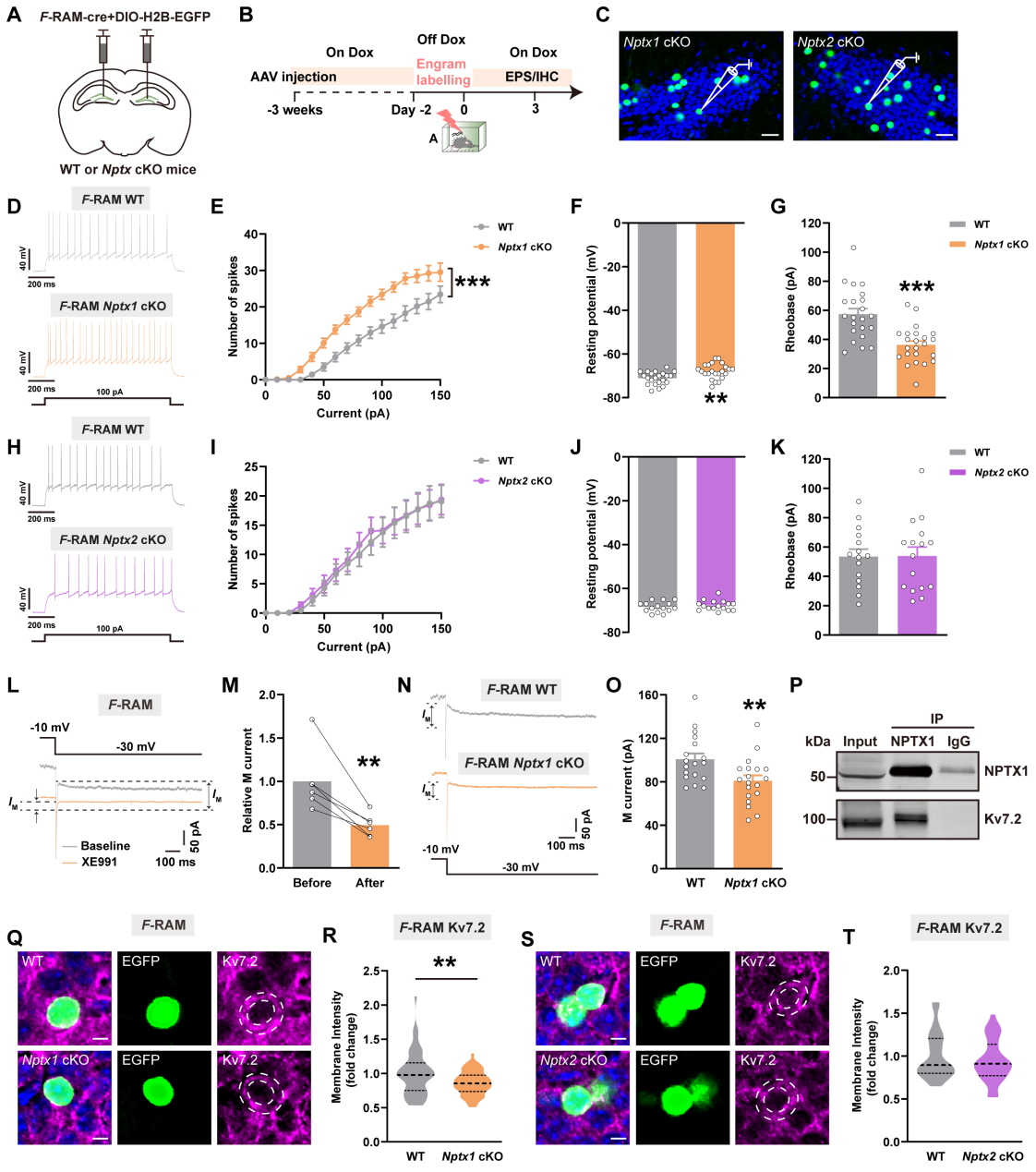
A
F-RAM-cre+DIO-H2B-EGFP
WT or Nptx cKO mice
B
On Dox
Off Dox
On Dox
AAV injection
Engram labelling
EPS/IHC
-3 weeks
Day -2
0
3
A
C
Nptx1 cKO
Nptx2 cKO
D
F-RAM WT
F-RAM Nptx1 cKO
40 mV
200 ms
100 pA
E
WT
Nptx1 cKO
Number of spikes
Current (pA)
***
F
Resting potential (mV)
**
G
Rheobase (pA)
***
H
F-RAM WT
F-RAM Nptx2 cKO
I
WT
Nptx2 cKO
Number of spikes
Current (pA)
J
Resting potential (mV)
K
Rheobase (pA)
L
F-RAM
-10 mV
-30 mV
Baseline
XE991
50 pA
100 ms
M
Relative M current
**
Before
After
N
F-RAM WT
F-RAM Nptx1 cKO
-10 mV
-30 mV
100 ms
50 pA
O
M current (pA)
**
WT
Nptx1 cKO
P
IP
kDa
Input
NPTX1
IgG
50
100
NPTX1
Kv7.2
Q
F-RAM
WT
EGFP
Kv7.2
Nptx1 cKO
R
F-RAM Kv7.2
**
Membrane Intensity (fold change)
WT
Nptx1 cKO
S
F-RAM
WT
EGFP
Kv7.2
Nptx2 cKO
T
F-RAM Kv7.2
Membrane Intensity (fold change)
WT
Nptx2 cKO

933

934

935 **Figure 2. The effects of *Nptx1* or *Nptx2* depletion on engram excitability and**
936 **membrane expression of Kv7.2.** (A) Diagram of AAV injection. (B) Experimental
937 scheme to label *F*-RAM, *N*-RAM engram ensembles. EPS: Electrophysiology, IHC:
938 Immunohistochemistry. (C) Representative expression of *F*-RAM engram cells in DG
939 of *Nptx1* and *Nptx2* cKO mice. Green: *F*-RAM engram cells of *Nptx1* and *Nptx2* cKO
940 mice, EGFP, Blue: DAPI. Scale bar: 20 μm. (D, H) Representative AP traces induced
941 by depolarizing current injections (100 pA) recorded from WT and *Nptxs* cKO mice.
942 (E) The input-output curves of AP spikes versus injected currents of WT and *Nptx1*
943 cKO mice. (F) The RMP of WT and *Nptx1* cKO mice. (G) The rheobase of WT and
944 *Nptx1* cKO mice. (I) The input-output curves of AP spikes versus injected currents of
945 WT and *Nptx2* cKO mice. (J) The RMP of WT and *Nptx2* cKO mice. (K) The rheobase
946 of WT and *Nptx2* cKO mice. (L) Representative traces of I_M current recorded before
947 and after application of XE991. (M) The normalized I_M current recorded at -30 mV
948 before and after application of XE991. (N) Representative traces of I_M current recorded
949 from WT and *Nptx1* cKO mice. (O) The average I_M current amplitudes recorded at -30
950 mV from WT and *Nptx1* cKO mice. (P) Immunoblotting of NPTX1 co-
951 immunoprecipitates with Kv7.2 in DG. (Q, S) Representative confocal images of
952 engram cells colocalizing with Kv7.2. Green: *F*-RAM engram cells, EGFP, Purple:
953 Kv7.2, Blue: DAPI. Dashed white lines outline cell membrane. Scale bar: 5 μm. (R)
954 The quantification of membrane Kv7.2 fluorescence intensity of WT and *Nptx1* cKO
955 neurons. (T) The quantification of Kv7.2 fluorescence intensity of WT and *Nptx2* cKO
956 neurons. Data are presented as mean ± S.E.M; $^{**}P < 0.01$, $^{***}P < 0.001$.
957

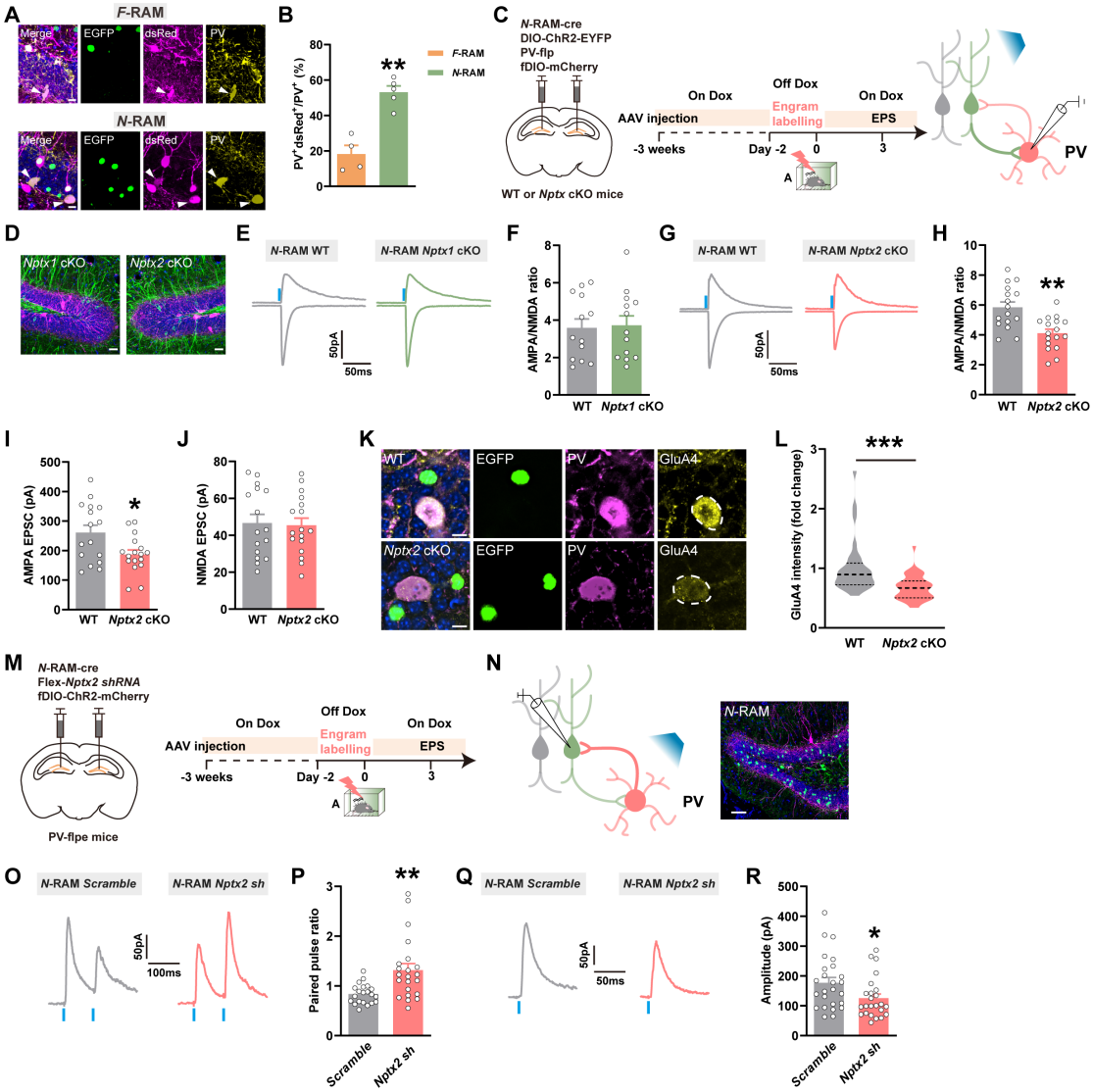
A
F-RAM
Merge
EGFP
dsRed
PV
N-RAM
B
PV+dsRed+/PV+ (%)
F-RAM
N-RAM
C
N-RAM-cre
DIO-ChR2-EYFP
PV-flp
fDIO-mCherry
WT or Nptx cKO mice
AAV injection
On Dox
Off Dox
Engram labelling
On Dox
EPS
-3 weeks
Day -2
0
3
PV
D
Nptx1 cKO
Nptx2 cKO
E
N-RAM WT
N-RAM Nptx1 cKO
50pA
50ms
F
AMPA/NMDA ratio
WT
Nptx1 cKO
G
N-RAM WT
N-RAM Nptx2 cKO
H
AMPA/NMDA ratio
WT
Nptx2 cKO
I
AMPA EPSC (pA)
WT
Nptx2 cKO
J
NMDA EPSC (pA)
WT
Nptx2 cKO
K
WT
EGFP
PV
GluA4
Nptx2 cKO
L
GluA4 intensity (fold change)
WT
Nptx2 cKO
M
N-RAM-cre
Flex-Nptx2 shRNA
fDIO-ChR2-mCherry
PV-flpe mice
AAV injection
On Dox
Off Dox
Engram labelling
On Dox
EPS
-3 weeks
Day -2
0
3
N
PV
N-RAM
O
N-RAM Scramble
N-RAM Nptx2 sh
50pA
100ms
P
Paired pulse ratio
Scramble
Nptx2 sh
Q
N-RAM Scramble
N-RAM Nptx2 sh
50pA
50ms
R
Amplitude (pA)
Scramble
Nptx2 sh

958
959

960 **Figure 3. The effects of *Nptx2* depletion on the functional connection between DG**
961 **local PV$^+$ interneurons and *N*-RAM ensemble.** (A) Representative confocal images
962 of DG local dsRed$^+$ cells immunostaining with PV. Green: EGFP, Purple: dsRed,
963 Yellow: PV, Blue: DAPI. White arrows indicate the dsRed$^+$ PV$^+$ colocalized cells. Scale
964 bar: 5 μm. (B) The percentages of colocalized cells in DG total PV$^+$ cells. (C) Diagram
965 of AAV injection and experimental scheme to label *N*-RAM engram ensembles. (D)
966 Diagram of representative expression of engram cells and PV$^+$ interneurons. Green: *N*-
967 RAM engram cells of *Nptx1* and *Nptx2* cKO mice, EYFP, Purple: PV$^+$ interneurons,
968 mCherry, Blue: DAPI. Scale bar: 10 μm. (E, G) Representative traces of opto-evoked
969 AMPA-EPSC and NMDA-EPSC recorded from WT and *Nptxs* cKO mice. (F) The
970 average A/N ratio recorded from WT and *Nptx1* cKO mice. (H) The average A/N ratio
971 recorded from WT and *Nptx2* cKO mice. (I, J) The average AMPA-EPSC and NMDA-
972 EPSC amplitudes recorded from WT and *Nptx2* cKO mice. (K) Representative confocal
973 images of GluA4 colocalizing with PV$^+$ interneurons. Green: *N*-RAM engram cells,
974 Purple: PV$^+$ interneurons, Yellow: GluA4. Scale bar: 10 μm. (L) The quantification of
975 GluA4 membrane expression on PV$^+$ interneurons in WT and *Nptx2* cKO mice. (M)
976 Diagram of AAV injection and experimental scheme to label *N*-RAM engram ensemble.
977 (N) Diagram of photostimulation and whole-cell patch clamp recordings (left) and
978 representative expression of *N*-RAM engram cells and PV$^+$ interneurons (right). Green:
979 *N*-RAM engram cells, EGFP, Purple: PV$^+$ interneurons, mCherry, Blue: DAPI. Scale
980 bar: 20 μm. (O, Q) Representative traces of opto-evoked PPR and oIPSC recorded from
981 *Scramble* and *Nptx2 shRNA* neurons. (P, R) The quantification of PPR and oIPSC

982 amplitudes recorded from *Scramble* and *Nptx2 shRNA* neurons. Data are presented as

983 mean ± S.E.M; *$P < 0.05$, **$P < 0.01$, ***$P < 0.001$.

984

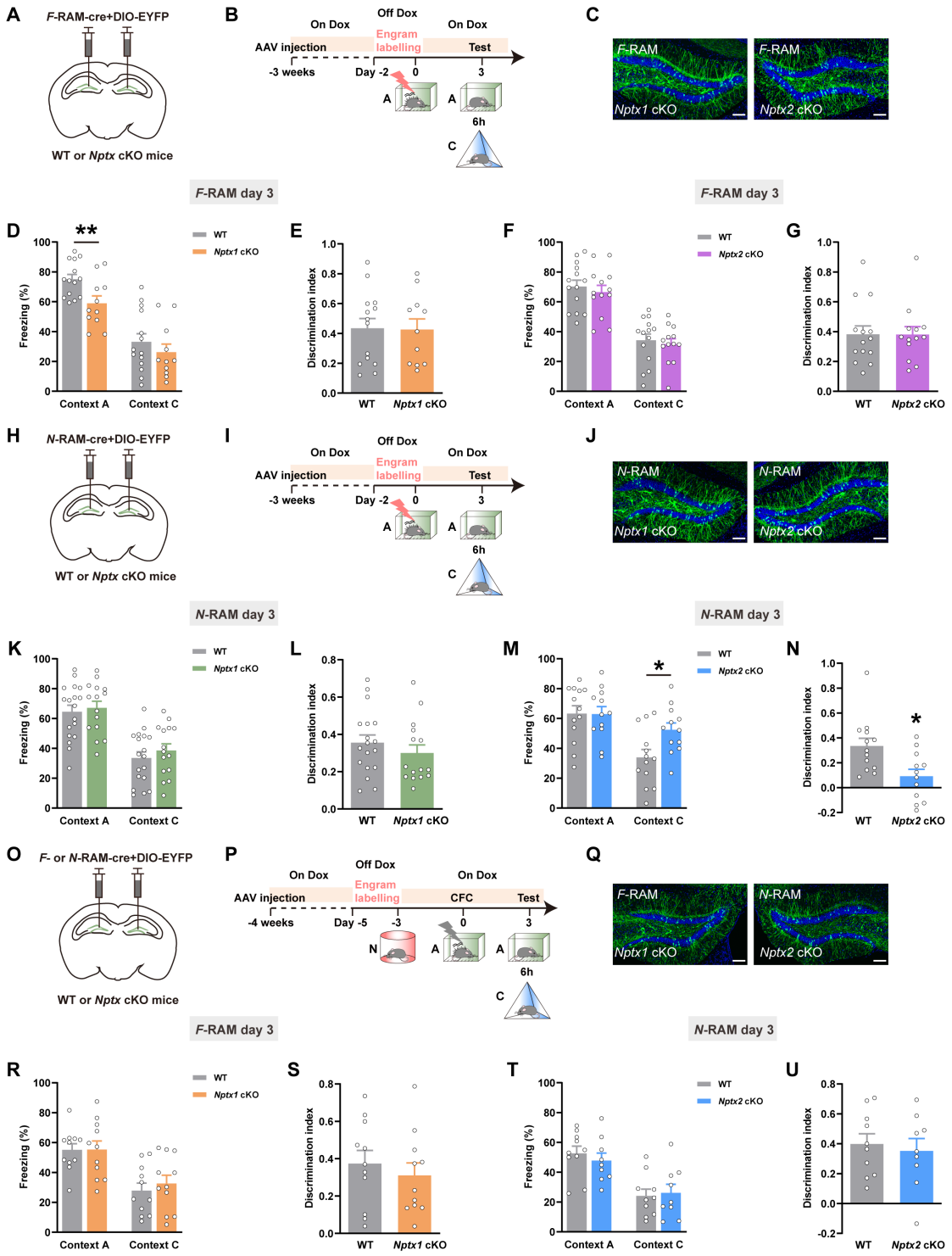
A
F-RAM-cre+DIO-EYFP
WT or Nptx cKO mice
B
On Dox
Off Dox
On Dox
AAV injection
Engram labelling
Test
-3 weeks
Day -2
0
3
A
A
6h
C
C
F-RAM
Nptx1 cKO
F-RAM
Nptx2 cKO
F-RAM day 3
F-RAM day 3
D
**
WT
Nptx1 cKO
Freezing (%)
Context A
Context C
E
Discrimination index
WT
Nptx1 cKO
F
WT
Nptx2 cKO
Freezing (%)
Context A
Context C
G
Discrimination index
WT
Nptx2 cKO
H
N-RAM-cre+DIO-EYFP
WT or Nptx cKO mice
I
On Dox
Off Dox
On Dox
AAV injection
Engram labelling
Test
-3 weeks
Day -2
0
3
A
A
6h
C
J
N-RAM
Nptx1 cKO
N-RAM
Nptx2 cKO
N-RAM day 3
N-RAM day 3
K
WT
Nptx1 cKO
Freezing (%)
Context A
Context C
L
Discrimination index
WT
Nptx1 cKO
M
*
WT
Nptx2 cKO
Freezing (%)
Context A
Context C
N
*
Discrimination index
WT
Nptx2 cKO
O
F- or N-RAM-cre+DIO-EYFP
WT or Nptx cKO mice
P
On Dox
Off Dox
On Dox
AAV injection
Engram labelling
CFC
Test
-4 weeks
Day -5
-3
0
3
N
A
A
6h
C
Q
F-RAM
Nptx1 cKO
N-RAM
Nptx2 cKO
F-RAM day 3
N-RAM day 3
R
WT
Nptx1 cKO
Freezing (%)
Context A
Context C
S
Discrimination index
WT
Nptx1 cKO
T
WT
Nptx2 cKO
Freezing (%)
Context A
Context C
U
Discrimination index
WT
Nptx2 cKO

985

986

Figure 4. The effects of *Nptxs* depletion in *F*-RAM and *N*-RAM ensembles on the expression of contextual fear memory. (A, H, O) Diagram of AAV injection. (B, I, P) Experimental scheme of CFC and memory retrieval. (C, J, Q) Representative expression of *F*- and *N*-RAM engram cells in DG. Green: *F*-RAM or *N*-RAM ensemble, EYFP, Blue: DAPI. Scale bar: 100 μm. (D, E) The freezing percentage and discrimination index of WT and *Nptx1* cKO mice tested in context A and context C at day 3 (*F*-RAM). (F, G) The freezing percentage and discrimination index of WT and *Nptx2* cKO mice tested in context A and context C at day 3 (*F*-RAM). (K, L) The freezing percentage and discrimination index of WT and *Nptx1* cKO mice tested in context A and context C at day 3 (*N*-RAM). (M, N) The freezing percentage and discrimination index of WT and *Nptx2* cKO mice tested in context A and context C at day 3 (*N*-RAM). (R, S) The freezing percentage and discrimination index of WT and *Nptx1* cKO mice tested in context A and context C at day 3 (*F*-RAM). (T, U) The freezing percentage and discrimination index of WT and *Nptx2* cKO mice tested in context A and context C at day 3 (*N*-RAM). Data are presented as mean ± S.E.M; $^{*}P < 0.05$, $^{**}P < 0.01$.

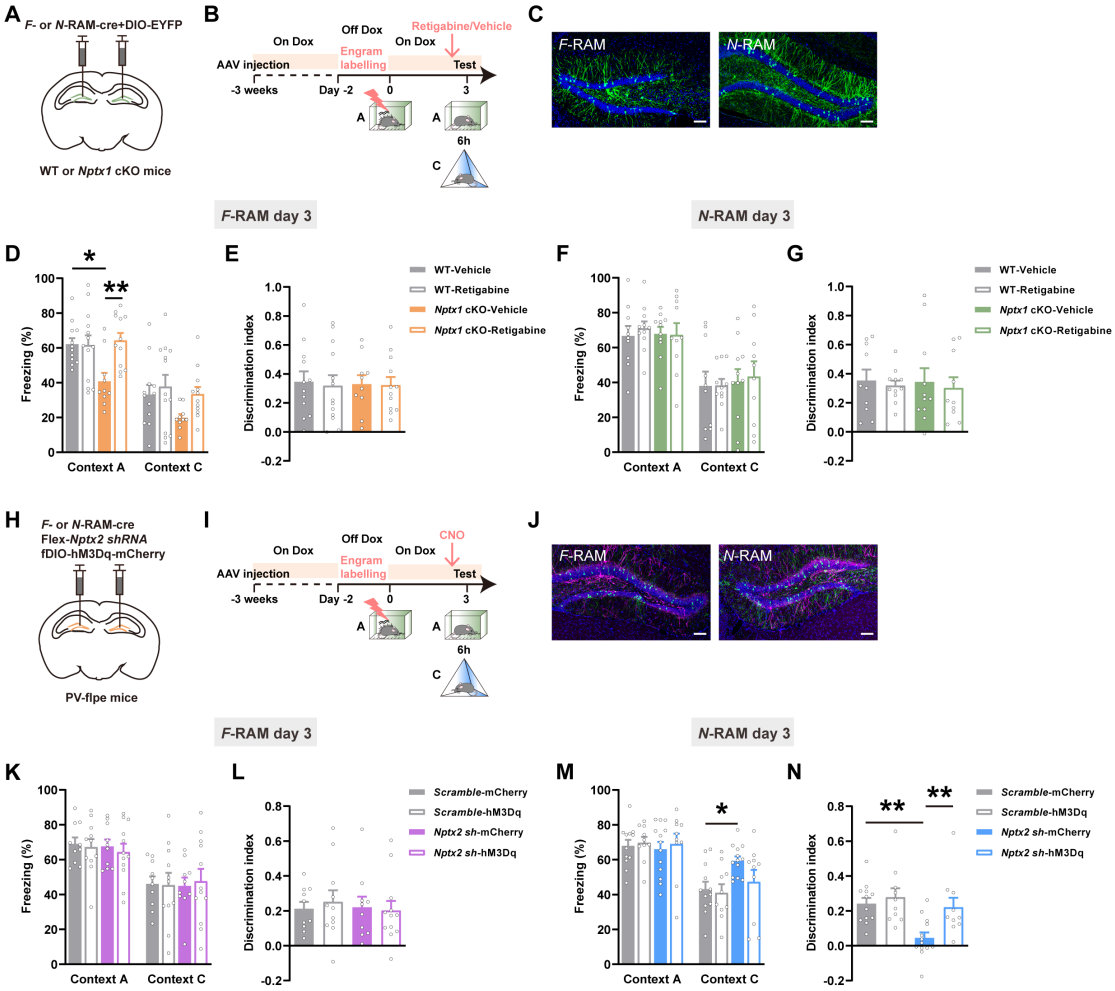
A
F- or N-RAM-cre+DIO-EYFP
WT or Nptx1 cKO mice
B
On Dox
Off Dox
On Dox
Retigabine/Vehicle
AAV injection
Engram labelling
Test
-3 weeks
Day -2
0
3
6h
C
F-RAM
N-RAM
F-RAM day 3
N-RAM day 3
D
Freezing (%)
Context A
Context C
E
Discrimination index
WT-Vehicle
WT-Retigabine
Nptx1 cKO-Vehicle
Nptx1 cKO-Retigabine
F
G
H
F- or N-RAM-cre
Flex-Nptx2 shRNA
fDIO-hM3Dq-mCherry
PV-flpe mice
I
CNO
J
K
L
Scramble-mCherry
Scramble-hM3Dq
Nptx2 sh-mCherry
Nptx2 sh-hM3Dq
M
N

1006 **Figure 5. The effects of activating Kv7.2 or DG PV$^+$ interneurons on memory**
1007 **deficits induced by *Nptxs* depletion in DG engram ensembles.** (A, H) Diagram of
1008 AAV injection. (B, I) Experimental scheme of memory retrieval test. (C) Representative
1009 images of *F*- and *N*-RAM engram cells in DG. Green: *F*-RAM and *N*-RAM ensembles,
1010 EYFP, Blue: DAPI. Scale bar: 100 μm. (D, E) The freezing percentage and
1011 discrimination index of WT-Vehicle, WT-Retigabine, *Nptx1* cKO-Vehicle and *Nptx1*
1012 cKO-Retigabine mice (*F*-RAM). (F, G) The freezing percentage and discrimination
1013 index of WT-Vehicle, WT-Retigabine, *Nptx1* cKO-Vehicle and *Nptx1* cKO-Retigabine
1014 mice (*N*-RAM). (J) Representative images of *F*- and *N*-RAM engram cells in DG.
1015 Green: *F*-RAM and *N*-RAM ensembles, EGFP, Purple: PV$^+$ interneurons, mCherry,
1016 Blue: DAPI. Scale bar: 100 μm. (K, L) The freezing percentage and discrimination
1017 index of *Scramble*-mCherry, *Scramble*-hM3Dq, *Nptx2 sh*-mCherry and *Nptx2 sh*-
1018 hM3Dq groups (*F*-RAM). (M, N) The freezing percentage and discrimination index of
1019 *Scramble*-mCherry, *Scramble*-hM3Dq, *Nptx2 sh*-mCherry and *Nptx2 sh*-hM3Dq
1020 groups (*N*-RAM). Data are presented as mean ± S.E.M; *$P < 0.05$, **$P < 0.01$.
1021
1022

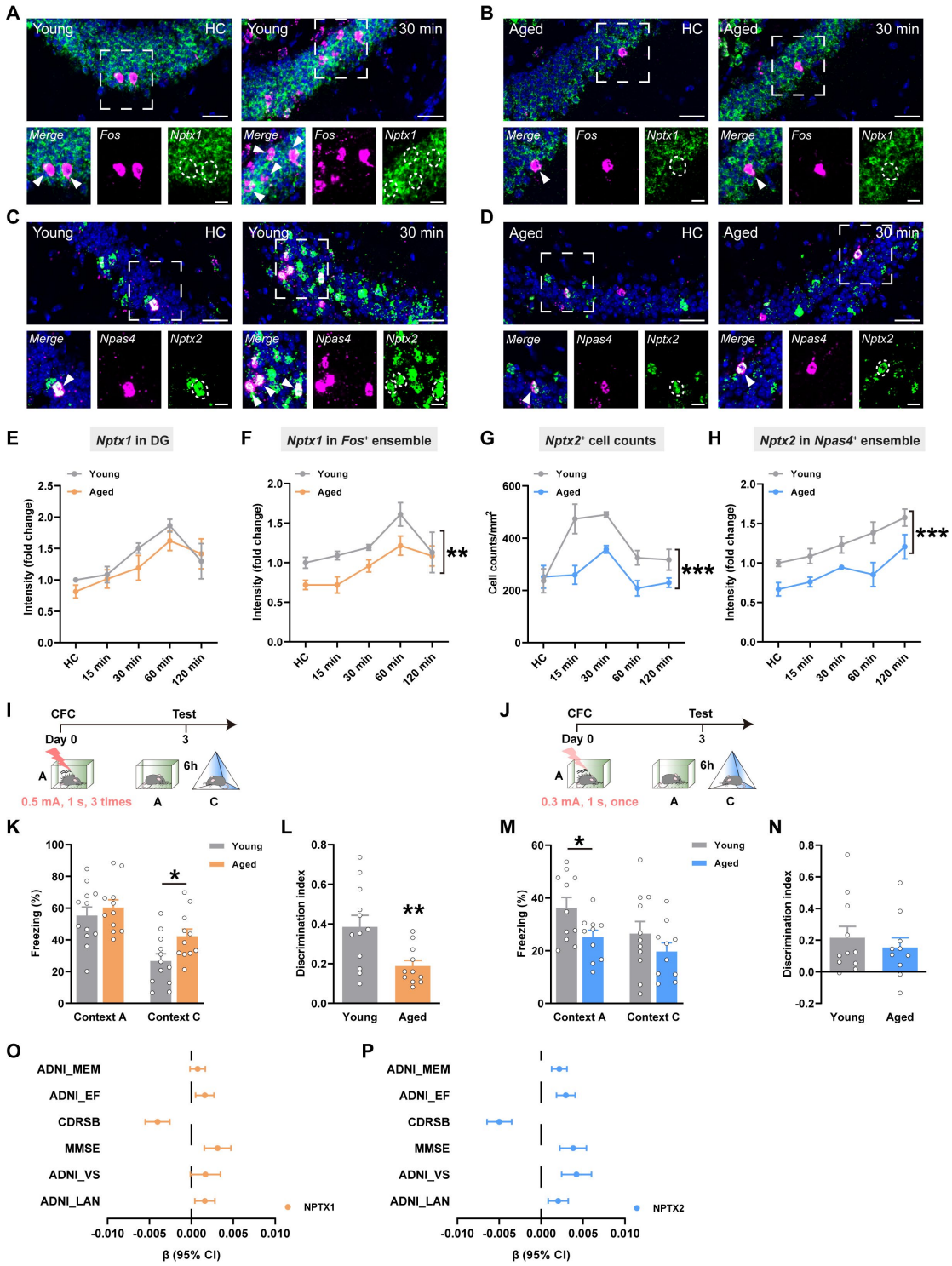
A
Young
HC
Young
30 min
Merge
Fos
Nptx1
B
Aged
HC
Aged
30 min
C
Young
HC
Young
30 min
Merge
Npas4
Nptx2
D
Aged
HC
Aged
30 min
E
Nptx1 in DG
F
Nptx1 in Fos+ ensemble
G
Nptx2+ cell counts
H
Nptx2 in Npas4+ ensemble
Young
Aged
Intensity (fold change)
Cell counts/mm2
HC
15 min
30 min
60 min
120 min
**
***
I
CFC
Test
Day 0
3
6h
A
C
0.5 mA, 1 s, 3 times
J
0.3 mA, 1 s, once
K
Freezing (%)
Context A
Context C
L
Discrimination index
Young
Aged
M
N
O
ADNI_MEM
ADNI_EF
CDRSB
MMSE
ADNI_VS
ADNI_LAN
NPTX1
β (95% CI)
P
NPTX2

1025 **Figure 6. *Nptxs* expression in DG engram cells, contextual fear memory in young**
1026 **and aged mice and the clinic correlation of NPTXs in human CSF with cognition.**
1027 (A, B) Representative confocal images of *Nptx1* colocalizing with *Fos* under HC
1028 condition and 30 min after CFC in DG of young and aged mice. Green: *Nptx1*, Purple:
1029 *Fos*, Blue: DAPI. White arrows indicate the colocalized cells. Scale bar: top, 30 μm,
1030 bottom, 10 μm. (C, D) Representative confocal images of *Nptx2* colocalizing with
1031 *Npas4* under HC condition and 30 min after CFC in DG of young and aged mice. Green:
1032 *Nptx2*, Purple: *Npas4*, Blue: DAPI. White arrows indicate the colocalized cells. Scale
1033 bar: top, 30 μm, bottom, 10 μm. (E) The fluorescence intensity of overall *Nptx1* mRNA
1034 in DG. (F) The fluorescence intensity of *Nptx1* mRNA in Fos^+ ensemble at HC, 15 min,
1035 30 min, 60 min and 120 min after CFC. (G) The $Nptx2^+$ cell counts in DG. (H) The
1036 fluorescence intensity of *Nptx2* mRNA in $Npas4^+$ ensemble at HC, 15 min, 30 min, 60
1037 min and 120 min after CFC. (I, J) Experimental scheme of CFC to test memory
1038 expression. (K, M) The freezing percentages of young and aged mice. (L, N) The
1039 discrimination indexes of young and aged mice. (O, P) Correlation of NPTXs with
1040 longitudinal changes of clinical cognitive scores including memory (MEM), executive
1041 function (EF), CDRSB, MMSE, visuospatial (VS) and language (LAN). Data are
1042 presented as mean ± S.E.M or β (95% CI); $*P < 0.05$, $**P < 0.01$, $***P < 0.001$.
1043
1044

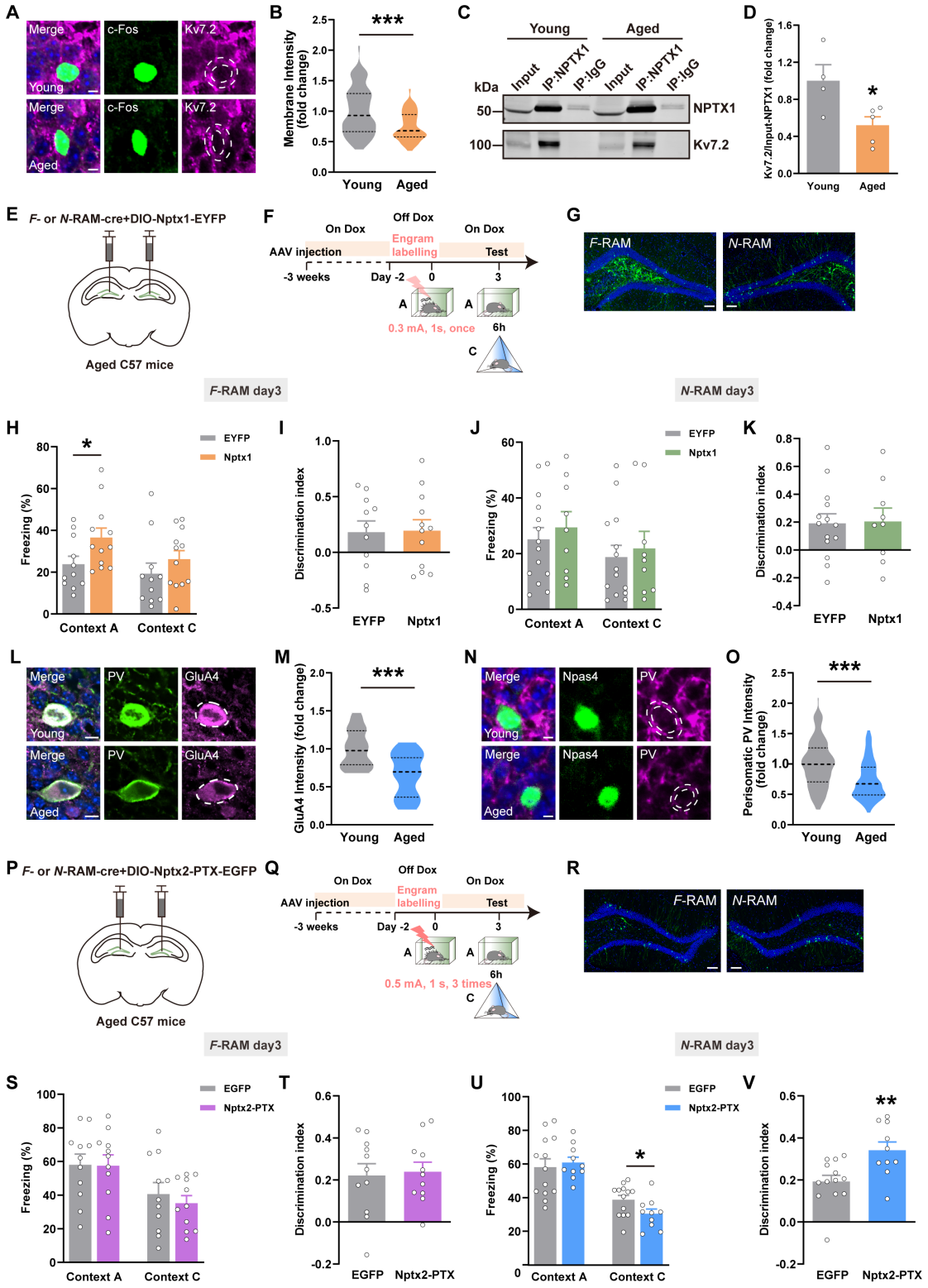
A
Merge
c-Fos
Kv7.2
Young
Aged
B
Membrane Intensity (fold change)
***
Young
Aged
C
Young
Aged
kDa
Input
IP:NPTX1
IP:IgG
50
100
NPTX1
Kv7.2
D
Kv7.2/Input-NPTX1 (fold change)
*
E
F- or N-RAM-cre+DIO-Nptx1-EYFP
Aged C57 mice
F
On Dox
Off Dox
On Dox
AAV injection
Engram labelling
Test
-3 weeks
Day -2
0
3
0.3 mA, 1s, once
6h
G
F-RAM
N-RAM
F-RAM day3
N-RAM day3
H
EYFP
Nptx1
Freezing (%)
Context A
Context C
I
Discrimination index
EYFP
Nptx1
J
Freezing (%)
Context A
Context C
K
Discrimination index
EYFP
Nptx1
L
Merge
PV
GluA4
Young
Aged
M
GluA4 Intensity (fold change)
***
Young
Aged
N
Merge
Npas4
PV
Young
Aged
O
Perisomatic PV Intensity (fold change)
***
Young
Aged
P
F- or N-RAM-cre+DIO-Nptx2-PTX-EGFP
Aged C57 mice
Q
On Dox
Off Dox
On Dox
AAV injection
Engram labelling
Test
-3 weeks
Day -2
0
3
0.5 mA, 1 s, 3 times
6h
R
F-RAM
N-RAM
F-RAM day3
N-RAM day3
S
EGFP
Nptx2-PTX
Freezing (%)
Context A
Context C
T
Discrimination index
EGFP
Nptx2-PTX
U
EGFP
Nptx2-PTX
Freezing (%)
*
Context A
Context C
V
Discrimination index
**
EGFP
Nptx2-PTX

1045

1046

1047 **Figure 7. Overexpression of NPTXs in DG engram ensembles rescued memory**
1048 **imprecision in aged mice.** (A) Representative confocal images of c-Fos$^+$ cells
1049 colocalizing with Kv7.2. Green: c-Fos$^+$ engram cells, Purple: Kv7.2, Blue: DAPI.
1050 Dashed white lines outline cell membrane. Scale bar: 5 μm. (B) The average membrane
1051 Kv7.2 fluorescence intensity of c-Fos$^+$ neurons in young and aged mice. (C)
1052 Immunoblotting of NPTX1 co-immunoprecipitates with Kv7.2 in DG of young and
1053 aged mice. (D) The quantification of IP-Kv7.2 in young and aged mice. (E, P) Diagram
1054 of AAV injection. (F, Q) Experimental scheme of memory retrieval test. (G, R)
1055 Representative expression of NPTX1 or NPTX2-PTX in *F*- or *N*-RAM engram cells in
1056 DG. Green: *F*-RAM or *N*-RAM ensemble, EYFP or EGFP, Blue: DAPI. Scale bar: 100
1057 μm. (H, I) The freezing percentage and discrimination index of EYFP and Nptx1 aged
1058 groups (*F*-RAM). (J, K) The freezing percentage and discrimination index of EYFP and
1059 Nptx1 aged groups (*N*-RAM). (L) Representative confocal images of GluA4
1060 colocalizing with PV$^+$ interneurons. Green: PV$^+$ interneurons, Purple: GluA4. Scale bar:
1061 10 μm. (M) The quantification of GluA4 membrane expression on PV$^+$ interneurons in
1062 young and aged mice. (N) Representative confocal images of PV neurites around
1063 Npas4$^+$ engram cells. Green: Npas4$^+$ engram cells, Purple: PV, Blue: DAPI. Dashed
1064 white lines outline PV neurites. Scale bar: 5 μm. (O) The average fluorescence intensity
1065 of PV neurites around Npas4$^+$ neurons in young and aged mice. (S, T) The freezing
1066 percentage and discrimination index of EGFP and Nptx2-PTX aged groups (*F*-RAM).
1067 (U, V) The freezing percentage and discrimination index of EGFP and Nptx2-PTX aged
1068 groups (*N*-RAM). Data are presented as mean ± S.E.M; *$P < 0.05$, **$P < 0.01$, ***$P <$

1069 0.001.